Reproduced by
NATIONAL TECHNICAL
INFORMATION SERVICE
Springfield, Va. 22151

D D C

DOUGLAS AIRCRAFT COMPANY

MCDONNELL DOUGLAS
CORPORATION

96

Reproduction in whole or in part is
permitted for any purpose of the
United States Government.

ACCESSION for
CFSTI
DDC
UNANNOUNCED
JUSTIFICATION
BY
DISTRIBUTION/AVAILABILITY
DIST. AVAIL.
A

CALCULATION OF VISCOUS DRAG AND TURBULENT BOUNDARY-LAYER SEPARATION ON TWO-DIMENSIONAL AND AXISYMMETRIC BODIES IN INCOMPRESSIBLE FLOWS

by

Tuncer Cebeci, G.J. Mosinskis, A.M.O. Smith

Report No. MDC J0973-01 November 1970

Prepared Under Contract N00014-70-C-0099

THIS RESEARCH WAS CARRIED OUT UNDER THE
NAVAL SHIP SYSTEMS COMMAND
GENERAL HYDROMECHANICS RESEARCH PROGRAM
SUBPROJECT SR 009 01 01, ADMINISTERED BY THE
NAVAL SHIP RESEARCH AND DEVELOPMENT CENTER

Approved for public release; distribution unlimited

Copy number | Report number MDC J0973-01

CALCULATION OF VISCOUS DRAG AND TURBULENT BOUNDARY-LAYER SEPARATION ON TWO-DIMENSIONAL AND AXISYMMETRIC BODIES IN INCOMPRESSIBLE FLOWS

Revision date | Revision letter

Issue date November 1970 | Contract number N00014-70-C-0099

Prepared by : Tuncer Cebeci
G. J. Mosinskis
A.M.O. Smith

Approved by :

A. E. Gentry, Chief
Applied Research Group
Aerodynamics Engineering

A. M. O. Smith
Chief Aerodynamics Engineer
Research

O. R. Dunn
Director of Aerodynamics

This research was carried out under the
Naval Ship Systems Command
General Hydromechanics Research Program
Subproject SR 009 01 01, administered by the
Naval Ship Research and Development Center

DOUGLAS AIRCRAFT COMPANY

MCDONNELL DOUGLAS CORPORATION

Approved for public release; distribution unlimited

1.0 SUMMARY

This report studies the accuracy of calculating the total drag of two-dimensional and axisymmetric bodies and the accuracy of calculating the location of turbulent boundary-layer separation in flows past such bodies.

The drag calculations were made by using the Douglas boundary-layer method. This is an implicit finite-difference method applicable to both laminar and turbulent boundary layers. The method also accounts for the transverse curvature effects. In general, comparison of calculated and experimental drag coefficients for both two-dimensional and axisymmetric bodies are in good agreement with experiment.

The separation calculations were made by considering four different separation-prediction methods. They are the Douglas boundary-layer method, Head's method, Stratford's method and Goldschmied's method. Comparisons of calculated and experimental results for several flows indicate that prediction of separation by the first three methods is quite good.

2.0 TABLE OF CONTENTS

		Page
1.0	Summary	1
2.0	Table of Contents	2
3.0	Index of Figures	4
4.0	Principal Notation	8
5.0	Introduction	11
6.0	Calculation of Viscous Drag of Two-Dimensional and Axisymmetric Bodies in Incompressible Flows	13
	6.1 Three Different Approaches for Calculating the Drag of Streamlined Bodies	14
	6.2 Modification of Douglas Boundary-Layer Method to Account for Flows at Low Reynolds Numbers	17
	6.3 Modification of Douglas Boundary-Layer Method to Account for the Streamwise Wall Curvature	24
	6.4 Prediction of Transition Point	25
	6.4.1 The Method of Michel	26
	6.4.2 The Method of Granville	29
	6.5 Procedure for Calculating Boundary-Layer Development About Streamlined Bodies	29
7.0	Comparison of Calculated and Experimental Drag Coefficients of Two-Dimensional and Axisymmetric Bodies	32
	7.1 Drag Coefficients of Two-Dimensional Bodies	34
	7.2 Drag Coefficients of Axisymmetric Bodies	43
8.0	Calculation of Turbulent Boundary-Layer Separation About Two-Dimensional and Axisymmetric Bodies in Incompressible Flows	55
	8.1 Methods for Predicting Turbulent Boundary-Layer Separation	55
	8.1.1 Head's Method	57
	8.1.2 Stratford's Method	59
	8.1.3 Goldschmied's Method	64

Page

9.0 Comparison of Calculated and Experimental Turbulent Boundary-Layer Separation in Two-Dimensional and Axisymmetric Bodies 66
9.1 Results for Schubauer's Elliptic Cylinder 67
9.2 Results for Roshko's Circular Cylinder 69
9.3 Results for Several Airfoils 71
9.4 Results for Axisymmetric Flows 72
10.0 Concluding Remarks 78
11.0 Future Work 82
12.0 Acknowledgments 86
13.0 References 87

3.0 INDEX OF FIGURES

No.	Title	Page
1	Boundary-layer flow along an airfoil	15
2	Variation of strength of wake component with Reynolds number	17
3	Comparison of calculated and experimental velocity distributions for turbulent flows at low Reynolds numbers [14]	20
4	Variation of mixing-length constant with Reynolds number	21
5	Variation of damping constant with Reynolds number	21
6	Comparison of local skin-friction coefficients for a flat-plate turbulent flow at low Reynolds number	22
7	Comparison of calculated and experimental skin-friction coefficients for the data of Schubauer and Klebanoff [20]. Calculations were made with and without the low Reynolds number modification	22
8	Comparison of calculated and experimental skin-friction coefficients for the data of Moses [20]	23
9	Comparison of calculated and experimental skin-friction coefficients for the data of Schubauer and Klebanoff [20]. Calculations were made with and without the curvature correction. The low Reynolds number correction was included in both cases	25
10.	Transition-correlation curves of Michel and Smith	27
11	Granville's transition-correlation curve	28
12	Variation of critical Reynolds number, R_{θ_i}, with shape factor according to stability theory	28
13	Comparison of calculated and experimental results for Newman's airfoil [20]	31
14	Velocity distribution near the trailing edge	33
15	Comparison of calculated and experimental drag values for the NACA $65_{(215)}$-114 airfoil at $C_\ell = 0.14$ [25]. Transition points were calculated by Michel's method	35
16	Calculated and experimental drag coefficients for the NACA 4412 airfoil [26,27]. Transition points were calculated by Michel's method	36

No.	Title	Page
17	Calculated and experimental drag coefficients for the NACA 64A010 airfoil [28]. Transition points were calculated by Michel's method	36
18	Comparison of calculated and experimental momentum thickness values for the upper surface of the RAE 101 airfoil [29]. Transition position was calculated by Michel's method	37
19	Calculated and experimental results for the NACA 63_3-018 airfoil [32]. Transition points were calculated by Michel's method	39
20	Comparison of calculated and experimental drag coefficients for the NACA 4412 airfoil [27]. The calculated drag coefficients were obtained by using Michel's and Granville's methods	41
21	The variation of θ_i/θ_a with r_0/δ for two values of n	45
22	Pressure distribution on DTMB body 4154 with and without viscous correction $R_L = 4 \times 10^6$	46
23	Variation of total drag coefficient with axial distance for the DTMB body 4154 at $R_L = 4 \times 10^6$ [34]. The total drag coefficient was calculated by using Granville's formula (7.14)	47
24	Comparison of calculated and experimental drag values for the DTMB body 4154 [34]. The total drag coefficients were obtained by using Granville's formula (7.14) and by taking the point where $C_p = 0$ as the tail end	48
25	Comparison of calculated and experimental results for the DTMB body 4165 [34]	49
26	Comparison of calculated and experimental results for the DTMB body 4159 [34]	49
27	Comparison of calculated and experimental results for the XZS2G-1 airship at $R_L = 188 \times 10^6$ [35]	50
28	Comparison of calculated and experimental drag values for the XZS2G-1 airship [35]. Total drag coefficients were obtained by Granville's formula (7.14)	51
29	Comparison of calculated and experimental results for the Murphy bodies of revolution [36]	52
30	Comparison of calculated and experimental velocity profiles for the Murphy bodies of revolution [36]	53

No.	Title	Page
31	Comparison of predicted and experimental separation points for Schubauer's elliptic cylinder at $R_D = 1.18 \times 10^5$ [43]	67
32	Comparison of calculated and experimental local skin-friction coefficients for Schubauer's elliptic cylinder [43]. The calculations were made by the Douglas boundary-layer method	68
33	Comparison of calculated and experimental velocity profiles for Schubauer's elliptic cylinder [43]. The calculations were made by the Douglas boundary-layer method	69
34	Comparison of predicted separation points with experiment for Roshko's circular cylinder [44]	70
35	Variation of shape factor with two pressure distributions per Roshko's circular cylinder [44]. Calculations were made by Head's method for $R_D = 8.4 \times 10^6$	71
36	Comparison of predicted separation points with experiment for the airfoil-like body of Schubauer and Klebanoff [45]	73
37	Comparison of predicted separation points with experiment for Newman's airfoil [39]	73
38	Predicted separation points for the experimental pressure distribution on the NACA 65(216)-222 airfoil [46]	74
39	Predicted separation points for the experimental pressure distribution on the NACA 4412 airfoil [26].	74
40	Predicted separation points for the experimental pressure distribution on the NACA 66,2-420 airfoil [30].	75
41	Predicted separation points for the experimental pressure distribution on the NACA 65,2-421 airfoil [47]. (a) Negative angles of attack. (b) Positive angles of attack	76
42	Variation of $C_{D_{exp}} - C_{D_{cal}}$ with angles of incidence for three airfoils.	79
43	Comparison of calculated and experimental results for two-dimensional bodies. The results are shown for 57 drag values at angles of incidence less than 6 degrees	80
44	Comparison of calculated and experimental wake profiles in adverse pressure gradients.	83

TABLES

No.	Title	Page
1	A comparison of calculated and experimental drag coefficients for the NACA 66,2-420 airfoil [30]	38
2	A comparison of calculated and experimental drag coefficients for the NACA 00-series	40
3	Comparison of calculated transition points and drag coefficients for the NACA 4412 airfoil at $R_L = 6 \times 10^6$	41
4	Comparison of calculated and experimental transition points and drag coefficients for the NACA $65_{(215)}$-114 airfoil at $C_\ell = 0.14$ [25]	42
5	Comparison of calculated and experimental drag coefficients for the Murphy bodies [36]	54
6	Comparison of calculated and experimental separation points for the bodies of revolution of Murphy [36]	72

4.0 PRINCIPAL NOTATION

A	damping length or frontal area, wherever applicable
A^+, A^{++}	damping constants
c	chord
c_f	local skin-friction coefficient, $\tau_w/(1/2)\rho u_e^2$
C_D	total drag coefficient
C_F	total skin-friction coefficient
C_ℓ	lift coefficient
C_p	pressure coefficient
D	maximum diameter
h	shape factor, θ_A/δ_A^*
H	shape factor, θ/δ^*
k	mixing-length constant
ℓ	mixing length
L	reference body length
n	exponent of power law velocity profile
p	pressure
p^+	pressure gradient parameter, Eq. (6.8)
r	radial distance from axis of revolution
r_o	local radius of body of revolution
R_c	chord-Reynolds number, $u_\infty c/\nu$
R_D	diameter-Reynolds number, $u_\infty D/\nu$
R_i	Richardson's number, Eq. (6.17)
R_L	length-Reynolds number, $u_\infty L/\nu$
R_o	maximum radius of body of revolution
R_x	local Reynolds number, $u_e x/\nu$

R_θ	Reynolds number, $(u_e\theta_{2-d})/\nu$
S	wall curvature term, Eq. (6.17)
u,v	x and y components of velocity, respectively
u',v'	fluctuating components of u and v, respectively
u*	friction velocity, $\sqrt{\tau_w/\rho}$
u^+	dimensionless velocity, u/u*
x	streamwise distance
y	distance normal to the surface of the body
y^+	dimensionless y-coordinate, yu^*/ν
α	angle of attack, or angle between y and r, wherever applicable
γ	intermittency factor, Eq. (6.10)
δ	boundary-layer thickness
δ^*	displacement thickness, $\int_0^\infty (1 - u/u_e)dy$
δ_A^*	displacement area, Eq. (7.9)
ε	eddy viscosity, $-\rho\overline{u'v'} = \rho\varepsilon \frac{\partial u}{\partial y}$
θ,θ_{2-d}	momentum thickness, $\int_0^\infty u/u_e\ (1 - u/u_e)dy$
θ_a	momentum area, Eq. (7.12)
θ_A	momentum area, Eq. (7.8)
$\bar{\lambda}_\theta$	Polhausen parameter, Eq. (6.19)
Λ	streamwise radius of curvature
μ	dynamic viscosity
ν	kinematic viscosity
ρ	density
τ	shear stress

ϕ	angle from stagnation point
Ψ	stream function

Subscripts

e	edge of the boundary layer
i	inner region
ℓ	lower surface
m	minimum pressure point
o	start of adverse pressure gradient, or outer region, wherever applicable
t	turbulent
tr	transition
u	upper surface
w	wall
∞	free-stream conditions

5.0 INTRODUCTION

Two very important problems in fluid mechanics are the prediction of viscous drag of a body and the location of flow separation, that is, the location at which the flow "stalls" or separates from the wall. Knowledge of these two quantities can be very useful in numerous problems. For example, an accurate prediction of the drag of a body can give a valuable insight into the performance of a vehicle or assist in the design of improved shapes. Likewise, a knowledge of the separation point is vital in many design problems of aerodynamics or hydrodynamics.

This report, which deals with the calculation of these two quantities in two-dimensional and axisymmetric flows, is written in fulfillment of the requirements of U.S. Navy Contract N00014-70-C-0099. The contract is a one-year "level-of-effort" type and the objectives are covered by the following work statement, taken from the contract.

1. Make a detailed study of calculation of total drag of two-dimensional and axisymmetric bodies by considering various computational schemes.

2. Review the available methods, together with the Douglas boundary-layer method [1] for predicting flow separation and investigate the accuracy of predicting separation in turbulent flows.

3. Check the results for both drag calculation and separation for a large number of test cases.

The present report describes the work accomplished during the contract. It also describes the further work that requires studying.

Sections 6 and 7 describe the drag calculations. Section 6 describes three possible approaches for calculating the total drag of two-dimensional and axisymmetric bodies and two transition-prediction methods. Section 7 presents comparisons of calculated and experimental drag coefficients. These calculations were made for a given pressure distribution by using the Douglas boundary-layer method described in reference 1. When the pressure distributions were not known experimentally, they were obtained by using the Douglas Neumann method [2].

Sections 8 and 9 describe the separation calculations. Section 8 presents a review of the four separation-prediction methods considered in this study, and Section 9 presents comparisons of calculated and experimental separation points for a number of flows.

Section 10 summarizes the results of drag and separation calculations and discusses the further work that should be done in this very important area.

6.0 CALCULATION OF VISCOUS DRAG OF TWO-DIMENSIONAL AND AXISYMMETRIC BODIES IN INCOMPRESSIBLE FLOWS

At high Reynolds numbers, the viscous drag of streamlined bodies is amenable to theoretical treatment and can be calculated by the boundary-layer theory [3-7]. According to this almost standard procedure, laminar and turbulent portions of the boundary layer along the body are calculated by methods which are generally of momentum integral type, and the location of the transition is calculated by an empirical method (if the transition is not known a priori). Then using boundary-layer parameters, such as momentum thickness, shape factor, and velocity ratio, all at the trailing edge of the body, the total drag of the body is calculated by a formula. For two-dimensional bodies, the total drag is usually computed by the Squire-Young formula [3]. For axisymmetric bodies, the total drag is computed either by Granville's formula [5] or by Young's formula [8]. These formulas are, in a way, a three-dimensional version of the Squire-Young formula.

In reference 4, Cebeci and Smith investigated the accuracy of a particular method for calculating the total drag of airfoils. This method consisted of the calculation of (1) pressure distribution by any suitable method, (2) laminar boundary-layer flow by Thwaites' method [9], (3) location of transition by Michel's method [10](if the transition is not known a priori), (4) turbulent boundary-layer flow by Head's method [11], and (5) total drag by means of the Squire-Young formula. That study showed that the method was quite accurate for predicting the total drag of airfoils except at very high Reynolds numbers . Because of the inaccuracy of Head's method used for turbulent boundary layer calculations, at high Reynolds numbers, the calculated drag values began to deviate from those of experimental values. For example, computed local skin-friction values and momentum thickness values for a turbulent flat-plate flow at various Reynolds numbers showed that the computed results agreed quite well with the experimental values at low Reynolds numbers, $R_\theta < 13{,}000$. On the other hand, at Reynolds numbers $R_\theta > 13{,}000$, the computed results began to deviate significantly from the experimental values.

The calculation of the total drag of bodies of revolution is somewhat more difficult than that of two-dimensional bodies for several reasons. First, the accuracy of the methods available for computing turbulent flows over bodies of revolution is not as well established as those of two-dimensional methods. [illegible] the available methods do not account for the transverse-curvature [illegible], which becomes quite important on slender bodies where the boundary-layer thickness can be of the same order of magnitude as the body radius. Third, the accuracy of calculating drag either by Young's or by Granville's formula has not been investigated thoroughly.

The drag calculations for both two-dimensional and axisymmetric bodies thus have one common feature: it is necessary to calculate the transition point (if it is not known a priori) and the boundary-layer growth as accurately as possible to make an accurate drag calculation. The boundary-layer method used in this report provides accurate boundary-layer calculations and eliminates most of the disadvantages of the methods discussed above. This method, which is based on the numerical solution of the boundary-layer equations in their differential form, is applicable to both laminar and turbulent flows. It has been well tested for both laminar and turbulent flows about two-dimensional and axisymmetric bodies including the effects of transverse curvature. In general, the method is found to be quite satisfactory [1,12,13].

In this report two transition prediction methods have been considered: those of Michel [10] and Granville [5]. The calculated drag values reported in reference 4 were obtained by using Michel's method. For this reason, in the present study Michel's method was used initially in order to compare the earlier drag results of reference 4 in which the boundary-layer calculations were made by using a combination of Thwaites' and Head's methods. By using Granville's method the drag of several airfoils was also computed and the results are compared with those obtained by Michel's method. The results are discussed in Section 7.

6.1 THREE DIFFERENT APPROACHES FOR CALCULATING THE DRAG OF STREAMLINED BODIES

In general, the flow around a streamlined body can be divided into four regions. Starting at the forward stagnation point A (see figure 1)there is at

Figure 1. Boundary-layer flow along an airfoil.

first a region in which the flow is laminar. After a certain distance, AB, which is mostly governed by the streamwise pressure gradient and Reynolds number, there is a region, BC, in which transition from laminar to turbulent flow takes place. In the third region, the flow from C to the trailing edge D is fully turbulent. Finally, at the trailing edge, the boundary layer of the upper surface joins that of the lower surface to form the turbulent wake*.

The total drag of a two-dimensional body such as the one shown in figure 1 is generally obtained by measuring its velocity profile in the wake of the body and using, for example, Jones' formula [3] which is given by

$$C_D = \frac{2}{c}\left(\frac{u_e}{u_\infty}\right)\int_0^\delta \frac{u}{u_e}\left\{1 - \left\{1 - \left(\frac{u_e}{u_\infty}\right)^2\left[1 - \left(\frac{u}{u_e}\right)^2\right]\right\}^{1/2}\right\}dy \tag{6.1}$$

This formula is usually applied to measured velocity profiles located at short distances behind the body.

The total drag can also be calculated theoretically by computing the boundary-layer development around the body. One popular approach uses the Squire-Young formula [3] given by

$$C_D = 2\left(\frac{\theta}{c}\right)_{T.E.}\left(\frac{u_e}{u_\infty}\right)_{T.E.}^{0.5(H_{T.E.}+5)} \tag{6.2}$$

*Here, we assume that the boundary layer does not separate from the surface.

According to (6.2) it is necessary to calculate the momentum thickness, θ, and shape factor, H, for a known velocity ratio u_e/u_∞ at the trailing edge. However, before these quantities at the trailing edge can be calculated, it is necessary to calculate the complete flow field, which is rather difficult.

Another way of calculating the drag is to extend the calculations into the wake and calculate the velocity profile in that region. This approach, although less empirical than the other, is much more difficult; the wake just behind the trailing edge is composed of two boundary layers back to back, and little is known about the way they interact or the accuracy of the turbulent calculations.

A third possibility for calculating the total drag is by computing the components of drag, namely, skin-friction drag and pressure drag, separately. The skin-friction drag can be obtained by the boundary-layer theory. For a given pressure distribution (whether it is experimental or theoretical does not make much difference, except possibly at the trailing edge), one can solve the governing boundary-layer equations, calculate the local skin-friction coefficient, and integrate it around the body to find the total skin-friction coefficient. For the pressure-drag calculations, however, it is necessary to know the experimental pressure distribution. In this case, the pressure forces can be resolved into chordwise and normal components. The sum of the latter forces gives the pressure drag. In case the experimental pressure distribution is not known, we can calculate the pressure distribution, say, by the Douglas Neumann method [2], and try to find the actual pressure distribution. This can be done by first calculating the displacement thickness around the body for the given pressure distribution. When the calculated displacement thickness distribution is added to the body coordinates, a new theoretical pressure distribution can be calculated by the boundary-layer theory. The iteration process continues until the change in the calculated pressure distribution is negligible.

In the present study the first approach is considered in detail and has been used to compute the drag of several two-dimensional and axisymmetric bodies. According to this approach the total drag of two-dimensional flows was computed by Squire-Young's formula or by Jones' formula. For axisymmetric flows, both Young's and Granville's formulas were used. The other two approaches have also

been studied but not as completely as the first approach. Because of the limited time available under the contract these studies were not finished.

6.2 MODIFICATION OF DOUGLAS BOUNDARY-LAYER METHOD TO ACCOUNT FOR FLOWS AT LOW REYNOLDS NUMBERS

Since an accurate calculation of boundary-layer development is essential for an accurate drag calculation, it is also necessary to investigate the accuracy of a turbulent boundary-layer method at low Reynolds numbers. Almost all the prediction methods for turbulent boundary layers, including the Douglas boundary-layer method, are based on empirical data obtained at high Reynolds numbers ($R_\theta > 6000$). According to several recent experiments [12-13], there is a definite Reynolds number effect for $R_\theta < 6000$. For example, in reference 14, Coles observed that his law of the wake formulation failed for low Reynolds numbers; the strength of the wake component, which stayed constant for momentum Reynolds numbers greater than 6000, showed a large variation at lower Reynolds numbers (see figure 2).

In the present study, such an effect becomes quite important when the drag of two-dimensional bodies is calculated at chord Reynolds numbers, R_c, ranging from 3 to 9 x 10^6. Usually, for such flows the momentum-thickness Reynolds number at transition is of the order of 500 to 1000. An accurate calculation of boundary layers at the trailing edge, and consequently, an

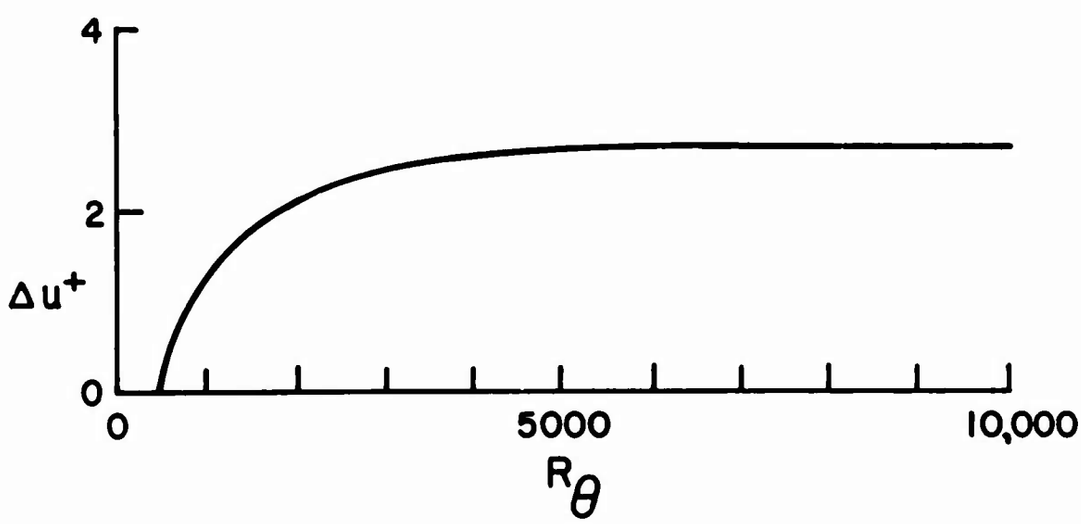

Figure 2. Variation of strength of wake component with Reynolds number.

accurate calculation of the drag by (6.2) depends upon the accuracy of calculating turbulent boundary layers from the point of transition. For this reason, studies were conducted in order to modify the present eddy-viscosity formulation to account for low Reynolds number flows. This was done as follows.

According to the present Douglas boundary-layer method the turbulent boundary layer is treated as a composite layer consisting of inner and outer regions. In the inner region, we use an eddy-viscosity expression that is based on Prandtl's mixing length theory; that is.

$$\epsilon_i = \ell^2 \left| \frac{\partial u}{\partial y} \right| \tag{6.3}$$

where ℓ, the mixing length, is given by $\ell = ky$. We use a modified expression for ℓ in (6.3) to account for the viscous sublayer and the transitional region close to the wall. This modification, suggested by Van Driest [17] for flat-plate flows, is

$$\ell = ky[1 - \exp(-y/A)] \tag{6.4}$$

where $k = 0.4$ and A is a damping length defined by $26\nu(\tau_w/\rho)^{-1/2}$. As it stands, it cannot be used for flows with pressure gradients and for flows with mass transfer. For this reason, the expression given by (6.4), which can also be written as

$$\ell^+ = ky^+[1 - \exp(-y^+/A^{++})] \tag{6.5}$$

was modified to account for flows with pressure gradient and mass transfer (see reference 18). This was done by defining A in terms of its friction velocity based on the sublayer thickness rather than its wall friction; that is,

$$A = 26\left(\frac{\tau_s}{\rho}\right)^{-1/2} \tag{6.6}$$

The sublayer friction velocity was obtained from the momentum equation approximated in the sublayer by the following equation

$$\frac{d\tau_s}{dy} - \frac{v_w}{\nu}\tau_s = \frac{dp}{dx} \tag{6.7}$$

The solution of (6.7) with $y^+ = 11.8$ enables the damping constant A^{++} to be written as

$$A^{++} = A^+ \left\{ -\frac{p^+}{v_w^+} [\exp(11.8v_w^+) - 1] + \exp(11.8v_w^+) \right\}^{-1/2} \tag{6.8}$$

where

$$p^+ = -\frac{dp}{dx} \frac{\nu}{\rho(u^*)^3}, \qquad A^+ = 26, \qquad v_w^+ = \frac{v_w}{u^*}$$

The expression for eddy viscosity in the outer region is based on a constant eddy viscosity

$$\varepsilon_o = 0.0168 \left| \int_0^\infty (u_e - u)dy \right| \tag{6.9}$$

modified by Klebanoff's intermittency factor γ, which is approximated by the following formula:

$$\gamma = \left[1 + 5.5 \left(\frac{y}{\delta} \right)^6 \right]^{-1} \tag{6.10}$$

It is important to recall at this point that the constants $k = 0.4$ and $A^+ = 26$ appearing in the inner eddy-viscosity expression were obtained for experimental data at high Reynolds numbers. For flows at low Reynolds numbers, they vary. One approach by which this variation can be obtained is the following:

Consider a flat-plate flow. Close to the wall, the momentum equation can be approximated by

$$\frac{d\tau}{dy} = 0$$

or

$$\tau = \tau_w \tag{6.11}$$

If we denote

$$\tau = \tau_\ell + \tau_t = \mu \frac{du}{dy} + \rho\varepsilon \frac{du}{dy} \tag{6.12}$$

and use (6.3) for ε with ℓ given by (6.4), it can be shown that (6.12) can be written as

$$\frac{du^+}{dy^+} = \frac{2}{1 + \left\{1 + 4k^2(y^+)^2\left[1 - \exp(-y^+/A^+)\right]^2\right\}^{1/2}} \tag{6.13}$$

Integrating (6.13) for various values of k and A^+ for a given R_θ-flow and comparing the results with the experimental data, one can easily obtain the variation of these constants with Reynolds number.

Figure 3 shows a comparison of calculated and experimental velocity distributions for various R_θ values for the experimental data of Simpson [14]

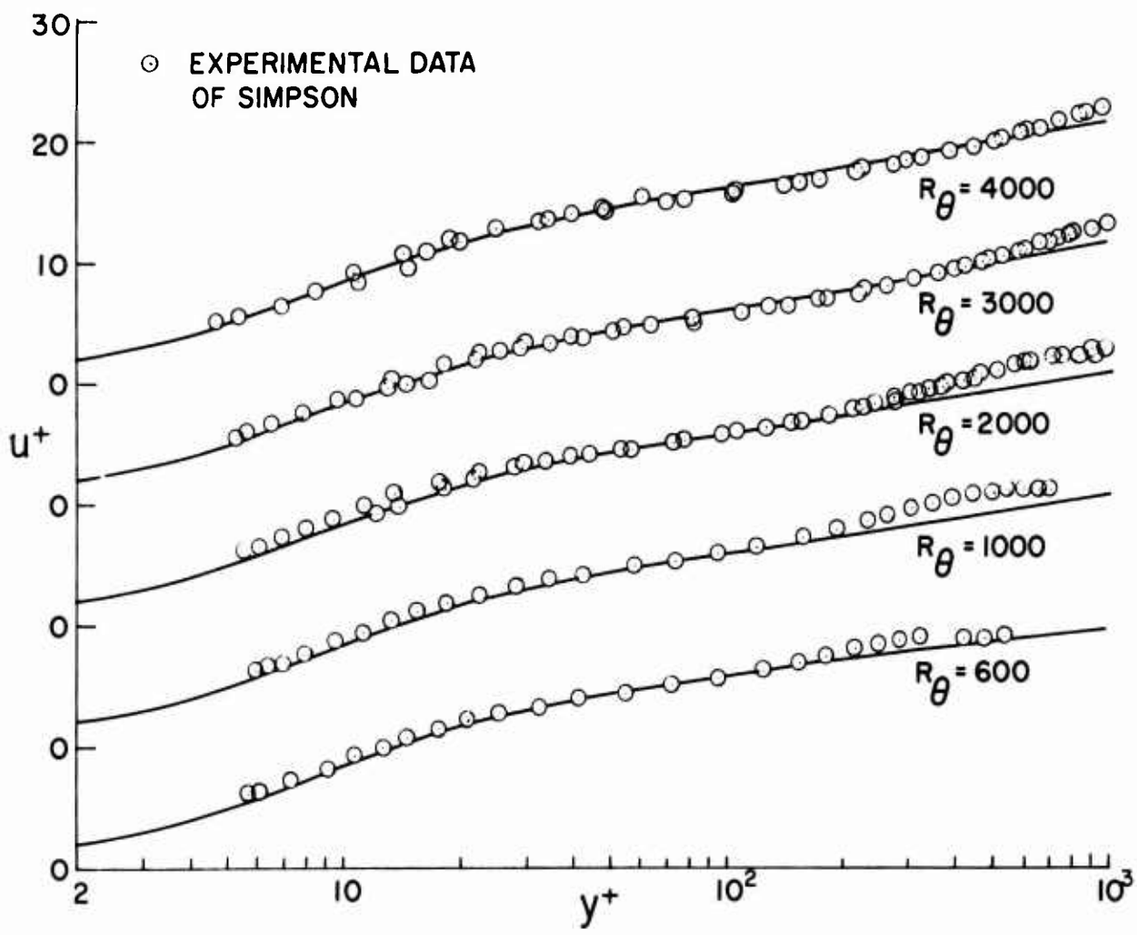

Figure 3. Comparison of calculated and experimental velocity distributions for turbulent flows at low Reynolds numbers.

which was taken at low Reynolds numbers. On the basis of this curve-fitting procedure, we find that k and A^+ can be satisfactorily expressed as functions of R_θ as shown in figures 4 and 5, respectively, and by the formulas that follow.

$$k = 0.40 + \frac{0.19}{1 + 0.49z^2} \qquad z \geq 0.3 \tag{6.14}$$

$$A^+ = 26 + \frac{14}{1 + z^2} \qquad z \geq 0.3 \tag{6.15}$$

where

$$z = 10^{-3}R_\theta$$

Figures 6 to 8 show comparisons of calculated skin-friction coefficients obtained by using the low Reynolds number correction with experimental results. Figure 6 compares the calculated c_f-values with those given by Coles' prediction [19] and the experimental values of Wieghardt [20]. Here the calculations were started as laminar at the leading edge and the flow was specified to be turbulent at the next x-station.

Figure 7 shows the results for Schubauer and Klebanoff's airfoil-like body designated as 2100 in reference 20. Again, the calculations were started as

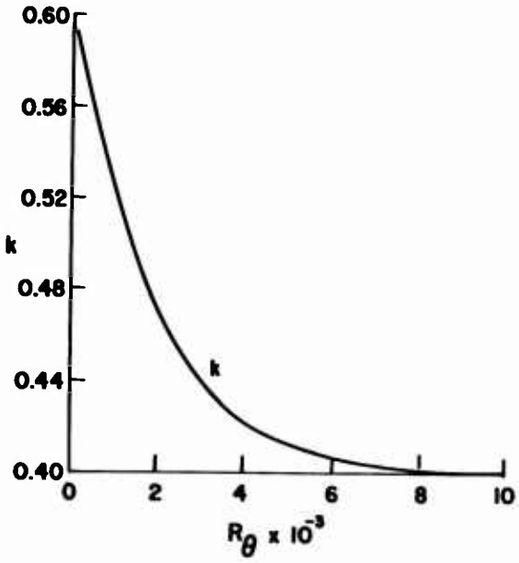

Figure 4. Variation of mixing-length constant with Reynolds number.

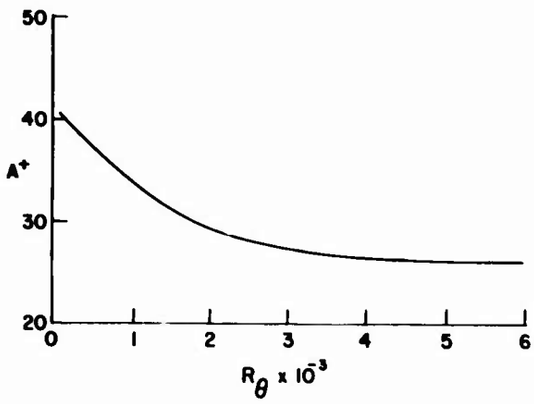

Figure 5. Variation of damping constant with Reynolds number.

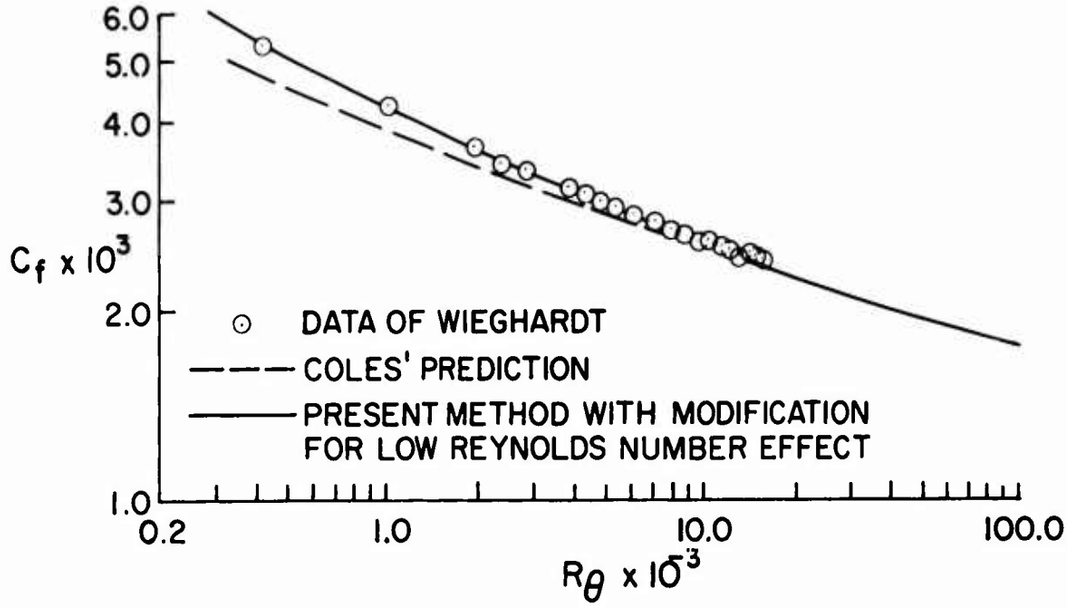

Figure 6. Comparison of local skin-friction coefficients for a flat-plate turbulent flow at low Reynolds number.

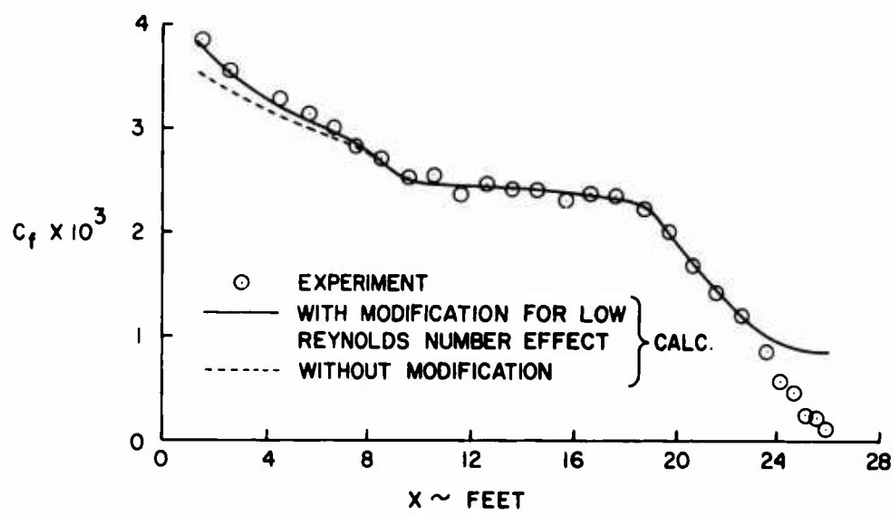

Figure 7. Comparison of calculated and experimental skin-friction coefficients for the data of Schubauer and Klebanoff [20]. Calculations were made with and without the low Reynolds number modification.

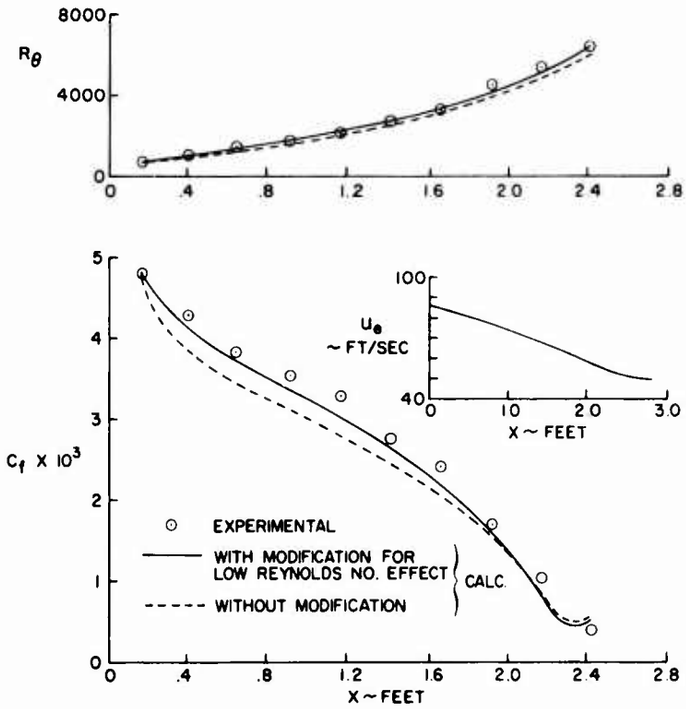

Figure 8. Comparison of calculated and experimental skin-friction coefficients for the data of Moses [20].

laminar at the leading edge and the flow was specified to be turbulent at the next x-station. Calculations with a flat-plate flow assumption continued until the experimental R_θ was matched. From this point on, we have used the experimental pressure distribution. The results show that when the Reynolds number is low ($R_\theta \doteq 8000$ at $x = 8$ feet) the modifications to the eddy-viscosity formulation improve the c_f-values.

Figure 8 shows the results for the experimental data of Moses designated as 3700 in reference 20. Here the calculations were started by using the experimental velocity profile. This flow is a low R_θ-flow. For example, at $x = 0.4$ feet, $R_\theta = 1000$, $x = 2.4$ feet $R_\theta = 6300$. As a result the improvement in calculated c_f-values is more pronounced than that of Schubauer and Klebanoff's data. Shown in the same figure is a comparison of calculated and experimental R_θ-values. Again the calculated results with the low Reynolds number correction agree better with the experimental data than those without this correction.

6.3 MODIFICATION OF DOUGLAS BOUNDARY-LAYER METHOD TO ACCOUNT FOR THE STREAMWISE WALL CURVATURE

Boundary-layer theory is based on the assumption that the pressure gradient normal to the wall can be neglected. If the wall has a streamwise curvature, this assumption is not always valid. This wall curvature may increase or decrease the intensity of the turbulent mixing depending on the wall curvature and can strongly affect the skin friction and heat transfer rates. For example, in reference 21 Thomann showed that the rate of heat transfer in a supersonic turbulent boundary layer on a concave wall was increased by the streamwise curvature of the wall. For the arrangement he investigated, the pressure was kept constant along the wall, and the increase of about 20 percent was therefore only due to the wall curvature. For a convex wall, he found a comparable decrease, also with constant pressure along the wall.

In this report we have attempted to make a correction to the present eddy-viscosity formulation in order to account for the wall curvature since such an effect can be quite important on thick airfoils and on the forward part of a blunt body. The expression suggested by Bradshaw [22] has been used. This expression is based on an analogy between streamline curvature and buoyancy in turbulent shear flows. With this wall curvature modification, the eddy-viscosity formulation becomes

$$\varepsilon_i = (ky)^2 \left[1 - \exp(-y^+/A^{++})\right]^2 \left(\frac{\partial u}{\partial y}\right)^2 S^2 \tag{6.16a}$$

$$\varepsilon_o = 0.0168 \left| \int_0^\delta (u_e - u)dy \right| \gamma S^2 \tag{6.16b}$$

where

$$S = \frac{1}{1 + 7R_i}, \qquad R_i = \frac{2u/\Lambda}{\partial u/\partial y} \tag{6.17}$$

The radius of curvature, Λ is positive for a convex surface $(\beta = 7)$ and is negative for a concave surface $(\beta = 0)$.

According to Bradshaw the effects of curvature on the mixing length or eddy viscosity are appreciable if the ratio of boundary-layer thickness δ to radius of curvature Λ exceeds roughly 1/300.

Figure 9 shows the effect of wall curvature modification on the computed c_f-values for the experimental data of Schubauer and Klebanoff [20]. In this case δ/Λ is around 1/150 and a correction such as the one given by (6.16) seems to improve the results.

6.4 PREDICTION OF TRANSITION POINT

One of the most important factors in the drag calculations is an accurate prediction of the transition point when it is not known experimentally. Probably the ideal way of predicting this point is to calculate the growth of the disturbances that build up in the boundary layer until they reach the condition at which transition is known to occur. Two strong factors that influence the position of transition are the streamwise pressure gradient and the turbulence in the freestream so that any calculation of the boundary-layer disturbance growth should account for them. However, because of the complexity of the problem, it has not, thus far, been possible to successfully account for such factors. Theoretical work has been limited largely to the criteria for stability of the boundary layer and the growth of small disturbances under particular flow conditions.

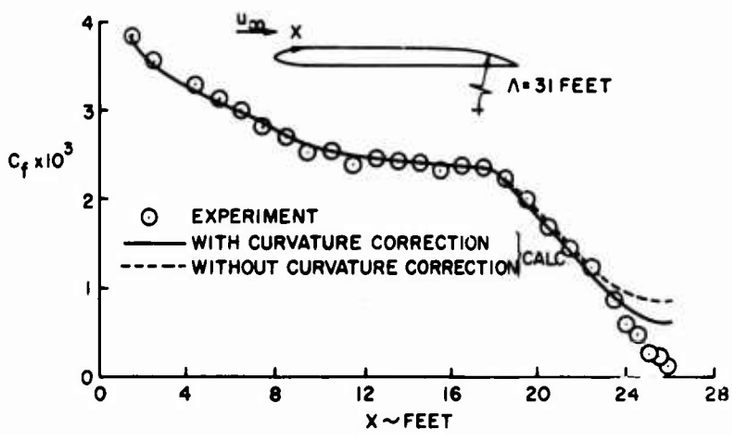

Figure 9. Comparison of calculated and experimental skin-friction coefficients for the data of Schubauer and Klebanoff [20]. Calculations were made with and without the curvature correction. The low Reynolds number correction was included in both cases.

At the present time there are several empirical methods for predicting the transition point. These are the method of Van Driest and Blumer, the method of Crabtree, the method of Granville, the method of Smith and Gamberoni, the method of Van Ingen and the method of Michel. In this report we consider two of these methods. They are the method of Michel[10] and the method of Granville [5]. These two methods are briefly described below.

6.4.1 The Method of Michel

Michel's method is based on the correlation of transition momentum-thickness-Reynolds number, $R_{\theta_{tr}}$, with x-Reynolds number, R_x. The reason for such a "universal" curve is mostly due to the data used in the correlation. The experimental results used in this correlation came from particular types of airfoils having similar pressure distributions and in such cases the values of R_θ and R_x would, to some extent, define a simple curve. Consequently, use of this method for airfoils with pressure distributions significantly different from the ones used in this correlation may introduce errors into the prediction of transition. In spite of this it is a useful relation.

As seen in figure 10, the range of the applicability of Michel's correlation is limited to values of R_x between 0.4×10^6 and 7×10^6. For this reason, in the present study we have used Smith's e^9-correlation curve [23] for values of R_x greater than 7×10^6. The resulting transition correlation curve may also be conveniently described by the following formula:

$$R_\theta = 1.174 \left(1 + \frac{22400}{R_x}\right) R_x^{0.46} \tag{6.18}$$

for

$$0.1 \times 10^6 \leq R_x \leq 60 \times 10^6$$

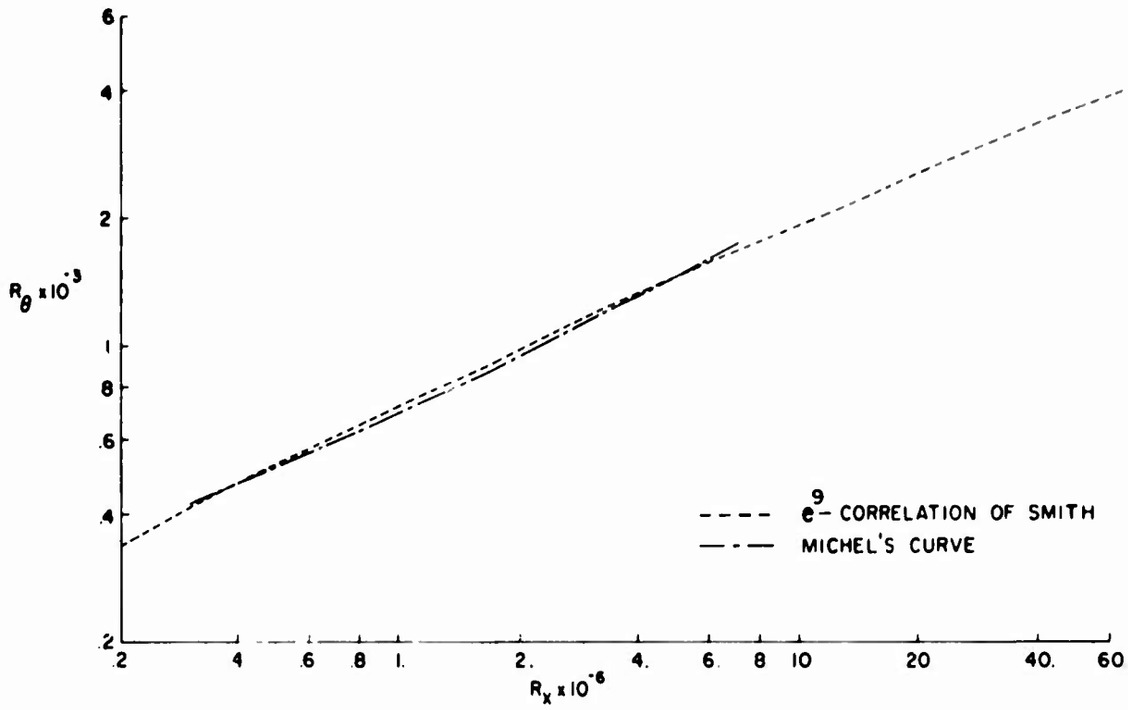

Figure 10. Transition-correlation curves of Michel and Smith

6.4.2 The Method of Granville

Granville's method consists of a single curve of $(R_\theta - R_{\theta_i})$ against the parameter $\overline{\lambda}_\theta$ as a transition criterion. See figure 11. The Polhausen parameter $\overline{\lambda}_\theta$ is defined as

$$\overline{\lambda}_\theta = \overline{\frac{\theta^2}{\nu}\frac{du_e}{dx}} = \frac{\int_{x_i}^{x} \theta^2/\nu(du_e/dx)dx}{x - x_i} \tag{6.19}$$

Granville, by using approximations of the same order as those used in Thwaites' method [9], reduced (6.19) to

$$\bar{\lambda}_\theta = \frac{4}{45} - \frac{1}{5}\left[\frac{R_\theta^2 - (u_e/u_{e_i})R_{\theta_i}^2}{R_x - (u_e/u_{e_i})R_{x_i}}\right] \tag{6.20}$$

To predict transition by Granville's method, it is necessary to calculate the critical momentum-Reynolds number, R_{θ_i}. This value can be calculated by using the curve given in figure 12. Once R_{θ_i} is known, then the values of $(R_\theta - R_{\theta_i})$ and $\bar{\lambda}_\theta$ are calculated from the point of instability, R_{x_i}, along the body until they intersect the universal transition curve given in figure 11.

Granville's method also accounts for the effects of free-stream turbulence on the transition point. However, it is restricted to flat-plate flows. Little is known about the effect of freestream turbulence on flows with pressure gradient. For this reason, we have neglected the freestream turbulence effect on transition point. It is believed that this assumption is a satisfactory one since flows for the bodies considered in this report were measured in low-turbulence tunnels.

For the cases studied in this report, Michel's method was initially used. The reason for this choice was to be able to make comparisons.

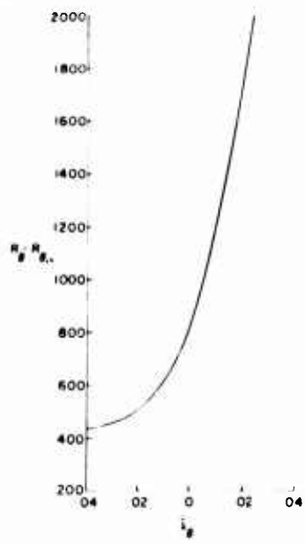

Figure 11. Granville's transition-correlation curve.

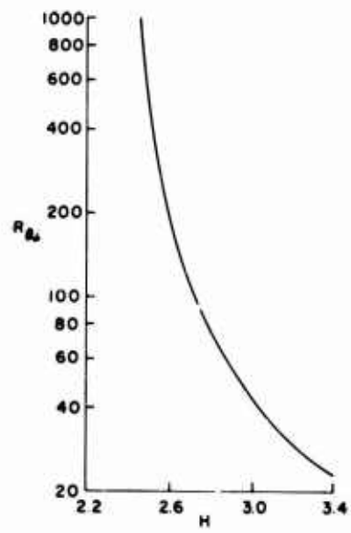

Figure 12. Variation of critical Reynolds number, R_{θ_i}, with shape factor according to stability theory.

between the results obtained by a previous study that utilized Michel's method [4]. However, in the present study we have also used Granville's method and made comparisons with those obtained by using Michel's method. These are discussed in Section 7.

The curves given in figures 11 and 12 are represented by the following equations:

$$R_\theta - R_{\theta_i} = \sum_{n=0}^{4} C_n \bar{\lambda}_\theta^n \qquad -0.04 \leq \bar{\lambda}_\theta \leq 0.024 \qquad (6.21)$$

where

$C_0 = 0.820571 \times 10^3$ $\qquad$ $C_3 = 0.516769 \times 10^7$

$C_1 = 0.282738 \times 10^5$ $\qquad$ $C_4 = 0.223023 \times 10^8$

$C_2 = 0.707219 \times 10^6$

$$R_{\theta_i} = \exp \sum_{n=0}^{7} C_n H^n \qquad 2.45 \leq H \leq 3.4 \qquad (6.22)$$

where

$C_0 = 493.906$ $\qquad$ $C_4 = -0.104478$

$C_1 = 407.017$ $\qquad$ $C_5 = -2.81454$

$C_2 = 53.9041$ $\qquad$ $C_6 = 0.355919$

$C_3 = 24.1642$ $\qquad$ $C_7 = 0.0120270$

6.5 PROCEDURE FOR CALCULATING BOUNDARY-LAYER DEVELOPMENT ABOUT STREAMLINED BODIES

In the calculation of drag of streamlined bodies according to any of the three approaches discussed in Section 6.1, it is necessary to calculate the complete boundary-layer development from the leading edge to the trailing edge. Let us consider the general case and assume that only the pressure distribution is given. This means that we need to calculate the laminar boundary-layer flow,

locate the position of transition, and then calculate the turbulent boundary layer. Each must be calculated to the same degree of accuracy if the drag calculations are to be as accurate.

In the results reported here, we have first calculated the laminar flow up to transition, which was assumed to take place at a point rather than in a region. Transition was computed by either Michel-Smith's transition-correlation curve or by Granville's method. Then at this point the turbulent flow calculations were started by activating the eddy-viscosity expressions in the governing boundary-layer equations and have continued the calculations up to the trailing edge. However, in some cases the calculations indicated laminar separation before the transition point was reached. In this case the wall shear became very small and prevented the solutions from converging. In such cases the laminar separation point was assumed to be the transition point and the turbulent flow calculations were started at that point.

It is also important to note that the computed boundary-layer parameters at the trailing-edge — momentum thickness in particular — showed a strong dependence on the streamwise spacing in the vicinity of the transition point unless the spacing is uniform. With uniform spacing, the dependence was removed and, at least for the cases studied in this report, consistent results were obtained.

The accuracy of calculating the complete boundary-layer development by the procedure that has been discussed was investigated for the experimental data of Newman [20]. The measurements, made on an airfoil, include experimental pressure distribution, transition point, and turbulent velocity profiles. The calculations were started at the leading edge. The experimental transition point was at $x = 1.169$ feet, but at $x = 1.009$ feet the calculations predicted laminar-flow separation. Consequently, the transition point was shifted to $x = 1.009$ feet. Calculations were made with and without the modification for low Reynolds number flow (e.g., at $x = 2.009$ feet, where the first experimental velocity profiles were reported, the R_θ-value was 5500) the calculated Reynolds number at transition is $R_\theta = 600$, and the calculated results show a slight improvement with this modification. See figure 13). But more important, when the calculations are started at $x = 2.009$

by using the initial experimental velocity profile, the results are almost exactly the same as those obtained by the modification. This is rather significant, since it shows that the present method is capable of calculating a complete boundary-layer development and gives justification for extending the calculation procedure to the drag calculations.

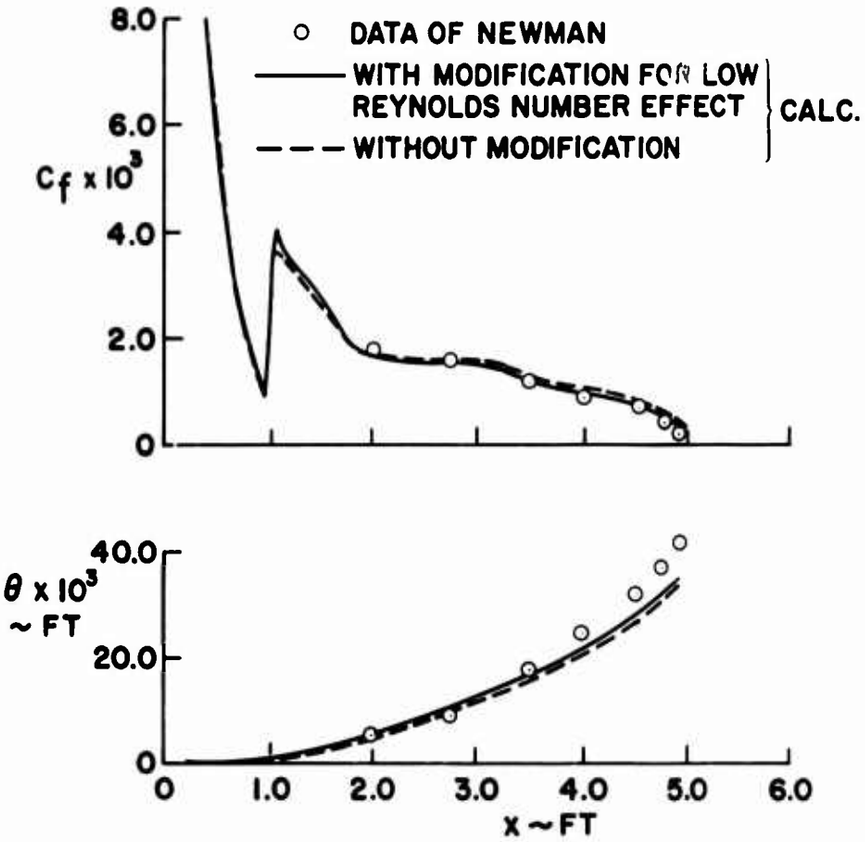

Figure 13. Comparison of calculated and experimental results for Newman's airfoil [20].

7.0 COMPARISON OF CALCULATED AND EXPERIMENTAL DRAG COEFFICIENTS OF TWO-DIMENSIONAL AND AXISYMMETRIC BODIES

In this section we present comparisons of calculated and experimental drag coefficients of several two-dimensional and axisymmetric bodies. The calculations were made by the procedure described in section 6.5. The drag coefficients, however, were calculated only by the first approach discussed in section 6.1. According to this approach, the drag of two-dimensional bodies was calculated by the Squire-Young formula and the drag of axisymmetric bodies by a three-dimensional version of this formula. Jones' formula was also used to compute the drag of two-dimensional bodies. In using this formula we used the velocity profiles at the trailing edge of the body and did not extend the calculations into the wake.

It is important to note at this time that use of either the Squire-Young formula or the Jones formula requires the value of (u_e/u_∞) at the trailing edge together with the boundary-layer parameters at the same location. If the experimental velocity distribution is used, this presents no problem in calculating the drag by these formulas since the velocity ratio is known at the trailing edge. However, with an inviscid velocity distribution these formulas are meaningless since one will always get a stagnation point at the trailing edge (for finite-trailing-edge angle). For this reason, when the inviscid velocity distribution is given, it becomes necessary to extrapolate the velocity distribution from the 95%-chord to the trailing edge. This procedure enables the calculations to be carried out up to and including the trailing edge. The error arising from this extrapolation of inviscid velocity distribution can be shown to be negligible as follows.

In reference 24 [p.182, eq.(9)], the expression for the drag coefficient C_D for both laminar and turbulent flow is

$$C_D = \left\{ \frac{1.422}{R_c^{3/5}} \left[\frac{u_{e_{tr}}}{u_\infty} \int_0^{x_{tr}/c} \left(\frac{u_e}{u_\infty}\right)^5 d\left(\frac{x}{c}\right) \right]^{3/5} + \frac{0.02429}{R_c^{1/5}} \int_{x_{tr}/c}^{1} \left(\frac{u_e}{u_\infty}\right)^4 d\left(\frac{x}{c}\right) \right\}^{5/6} \quad (7.1)$$

Now, consider only the contribution of the turbulent flow. Then

$$C_D = \left[\frac{0.02429}{R_c^{1/5}} \int_{x_{tr}/c}^{1} \left(\frac{u_e}{u_\infty}\right)^4 d(x/c) \right]^{5/6} \tag{7.2}$$

Assume that the velocity distribution between the 95%-chord point and the trailing edge is linear (fig. 14). Then the velocity distribution is given by

$$u_e/u_\infty = a + 20(b - a)(x/c - 0.95) \qquad 0.95 \leq x/c \leq 1 \tag{7.3}$$

where a is the value of the velocity at the 95%-chord point, and b is the value of the velocity at the trailing edge. Since Eq. (7.2) can be written as

$$C_D = \left[\frac{0.02429}{R_c^{1/5}} \int_{x_{tr}/c}^{0.95} \left(\frac{u_e}{u_\infty}\right)^4 d\left(\frac{x}{c}\right) + \frac{0.02429}{R_c^{1/5}} \int_{0.95}^{1} \left(\frac{u_e}{u_\infty}\right)^4 d\left(\frac{x}{c}\right) \right]^{5/6} \tag{7.4}$$

the term

$$C_{D_E} = \frac{0.02429}{R_c^{1/5}} \int_{0.95}^{1} \left(\frac{u_e}{u_\infty}\right)^4 d\left(\frac{x}{c}\right) \tag{7.5}$$

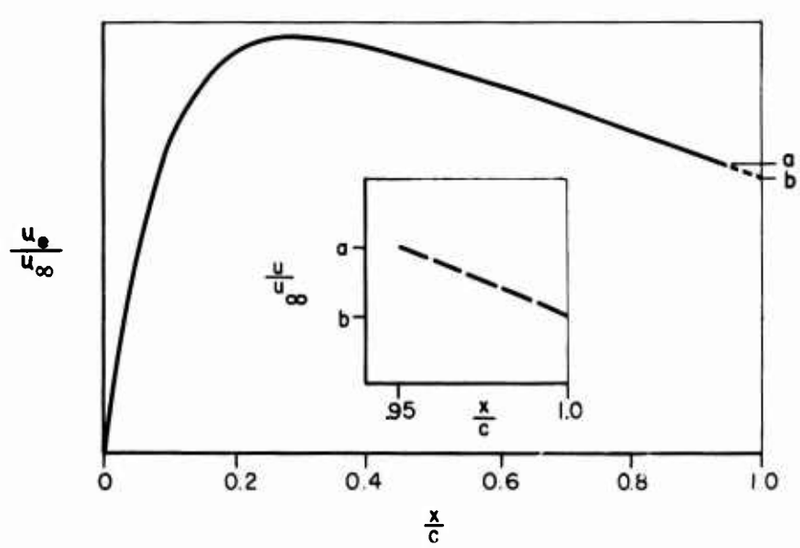

Figure 14. Velocity distribution near the trailing edge.

can be considered to be a "correction" or error term (assuming the exponent $5/6 \approx 1$) if we make an assumption for the velocity distribution between the 95%-chord point and the trailing edge. Substituting the expression for the velocity ratio from (7.3) into (7.5) and integrating gives an estimate of this quantity

$$C_{D_E} = (2.429/R_c^{1/5})10^{-4}\ (b^4 + ab^3 + a^2b^2 + a^3b + a^4) \tag{7.6a}$$

For $b = a$ (7.6a) becomes

$$C_{D_E} = (5 \times 2.429/R_c^{1/5})10^{-4}a^4 \tag{7.6b}$$

If $a = 1$ and $R_c = 10^6$, the correction term is approximately 5×10^{-5}, which is relatively small. At higher chord Reynolds numbers, the correction term becomes even smaller. Thus, extrapolating the inviscid velocity distribution to the trailing edge in the manner done in this study is justified.

7.1 DRAG COEFFICIENTS OF TWO-DIMENSIONAL BODIES

In most of the two-dimensional bodies considered in this report, the position of transition was not known and was calculated by using either Michel's or Granville's method. At first, the drag of a number of airfoils in which transition was obtained by Michel's method was calculated. These values were compared with those obtained in a previous study [4] in which transition was again calculated by Michel's method but the boundary-layer calculations were made by a combination of Thwaites' and Head's methods. After these comparisons, some of the calculations were repeated with Granville's transition-prediction method and in this way the effects of different transition prediction methods on drag were studied. Results obtained by using Michel's method are presented first.

Figure 15 shows the results for the NACA $65_{(215)}$-114 airfoil [25] at chord Reynolds numbers varying from 6×10^6 to 40×10^6 together with the calculated results obtained earlier [4]. The drag values which were obtained by using the Douglas boundary-layer method show a marked improvement over earlier results, which were obtained by using a combination of Thwaite's

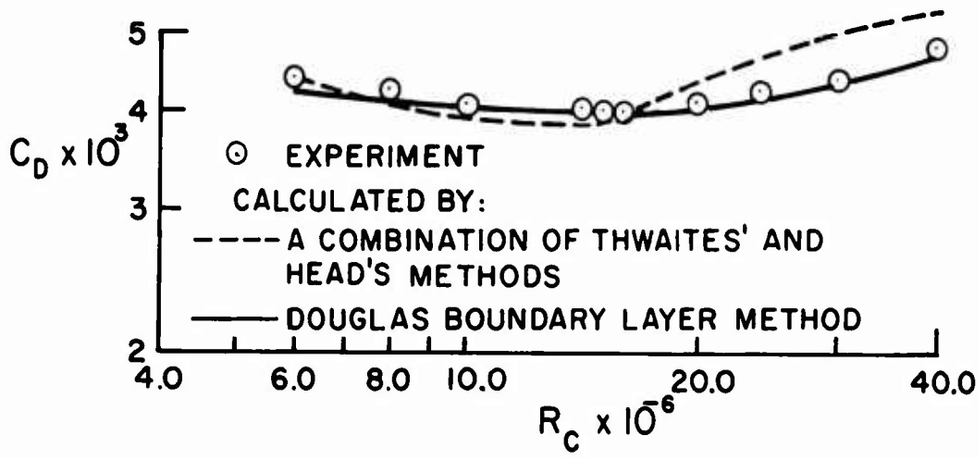

Figure 15. Comparison of calculated and experimental drag values for the NACA 65(215)-114 airfoil at $C_\ell = 0.14$ [25]. Transition points were calculated by Michel's method.

laminar boundary-layer method and Head's turbulent boundary-layer method. This is quite significant since, although good agreement was obtained at lower Reynolds numbers ($R_c < 9 \times 10^6$) according to the study described in reference 4, the agreement was poor at high Reynolds numbers, and the discrepancy was attributed to the inaccuracy of calculating turbulent boundary layers at high Reynolds numbers.

Figure 16 shows a comparison of calculated and experimental drag coefficients for the NACA 4412 airfoil at various lift coefficients. The experimental pressure distribution was given for $R_c = 3.1 \times 10^6$ for a wide range of angles of attack [26]. The experimental drag values were obtained from reference 27. However, the unseparated flow ranged from $\alpha = -6$ to $\alpha = 8^0$. For this reason, calculations were made for angles of attack of -6, -4, -2, 0, 2, 4 and 8 degrees for three chord-Reynolds numbers 3×10^6, 6×10^6, and 9×10^6 using the same experimental pressure distribution. Transition data was not given. Although not shown in this report, it is important to note that a comparison of present calculations with those that were obtained earlier [4] shows that the present drag values are in much better agreement with experiment.

Figure 17 shows the results for the NACA 64A010 airfoil. In this case the pressure distributions were given for a slightly compressible flow

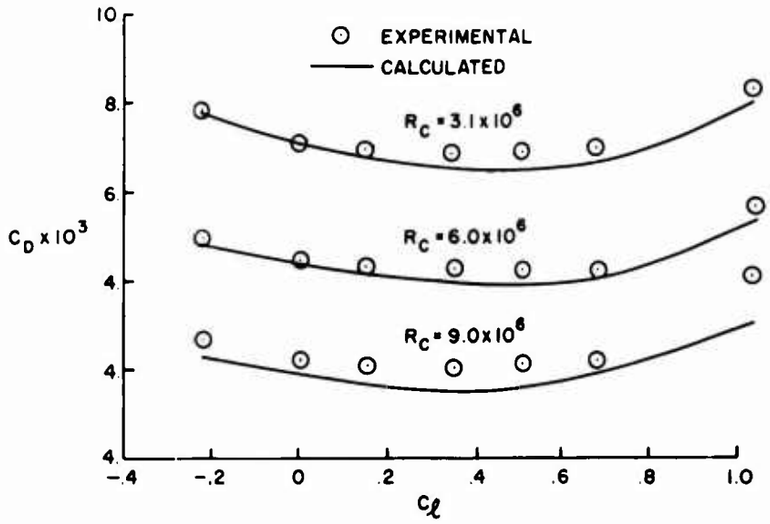

Figure 16. Calculated and experimental drag coefficients for the NACA 4412 airfoil [26,27]. Transition points were calculated by Michel's method.

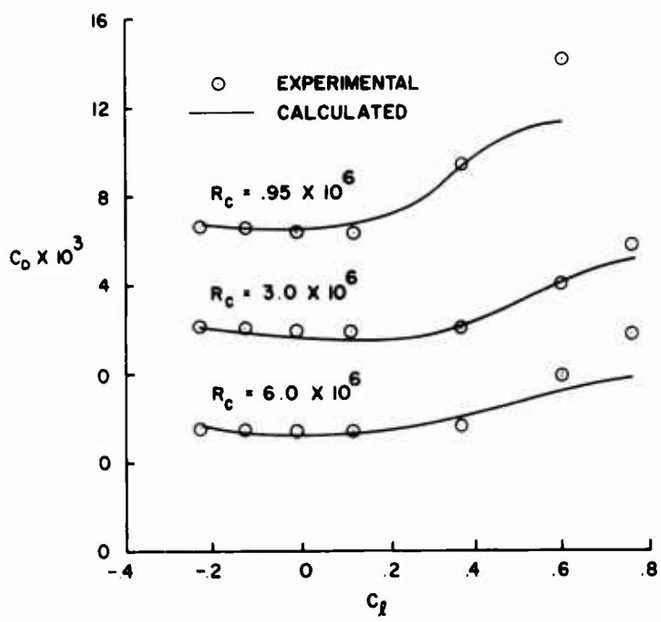

Figure 17. Calculated and experimental drag coefficients for the NACA 64A010 airfoil [28]. Transition points were calculated by Michel's method.

(M_∞ = 0.3) at $R_c = 0.95 \times 10^6$ [28] for an airfoil with 6-inches chord, for angles of attack up to and including stall. The calculations were made for three-chord Reynolds numbers, $R_c = 0.95 \times 10^6$, 3×10^6 and 6×10^6 for angles of attack of α = -1.8, -0.8, 0.2, 1.2, 2.2, 4.2 6.2 and 8.2. It is important to note that at higher angles of attack, it was necessary to input the experimental pressure distribution near the nose in considerable detail because of the high C_p values. This was done by fairing a curve through the available experimental points in that region.

Figure 18 shows a comparison of calculated and experimental momentum-thickness values [29] for the RAE 101 airfoil for a chord Reynolds number of $R_c = 1.6 \times 10^6$. The calculations were made for two angles of attack, $\alpha = 0^\circ$ and 4.09°. In the calculations the experimental pressure distribution was used. The total drag values of this airfoil were not given. For this reason, comparisons were limited to values of momentum-thickness only.

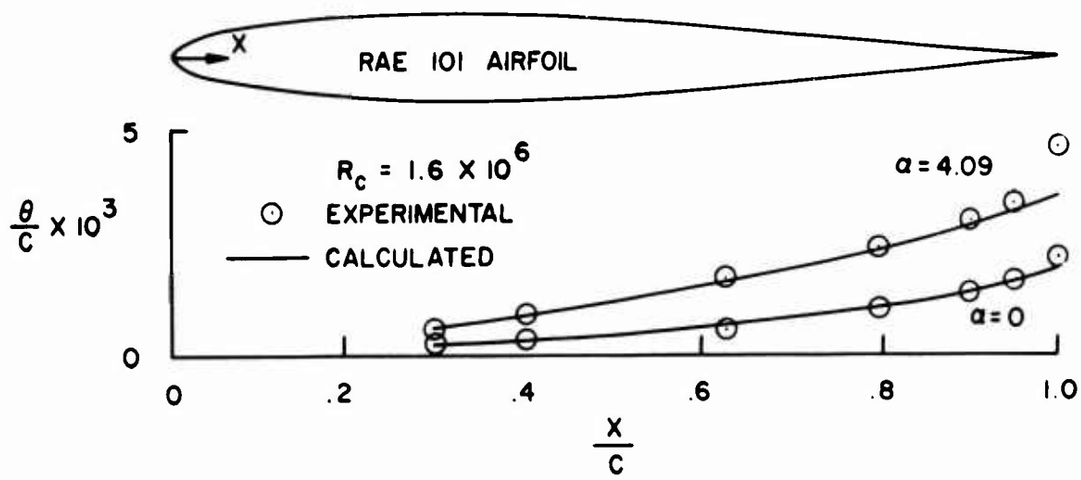

Figure 18. Comparison of calculated and experimental values of momentum thickness for the upper surface of RAE 101 airfoil [29]. Transition position was calculated by Michel's method.

Comparison of calculated and experimental drag coefficients were also made for the NACA 66,2-420 airfoil [30] at zero angle of attack. The calculations were made for three chord Reynolds numbers, $R_c = 6.67 \times 10^6$, 9.30×10^6 and 11.30×10^6 in which the experimental free-stream Mach number was 0.194, 0.269 and 0.385, respectively. In the calculations the experimental pressure distribution, which was obtained at $M_\infty = 0.194$, was used. In addition, in the calculations it was necessary to extrapolate the experimental pressure distribution to the trailing edge because the experimental pressure distribution was given only up to the 90%-chord point. The boundary layer was tripped at 10%-chord point, and the total drag coefficients for the three Reynolds numbers were obtained from wake measurements. A comparison of the calculated and experimental results is given in Table 1.

Table 1

A COMPARISON OF CALCULATED AND EXPERIMENTAL DRAG COEFFICIENTS FOR THE NACA 66,2-420 AIRFOIL [30]

$R_c \times 10^{-6}$	$C_{D_{exp}} \times 10^3$	$C_{D_{cal}} \times 10^3$
6.67	10.85	9.57
9.30	10.65	9.02
11.30	10.70	8.74

Calculations were also made for the NACA 35-215 airfoil [31]. For this airfoil, the total drag coefficient of the upper surface was calculated for a pressure distribution obtained from reference 31 at a chord Reynolds number of 26.7×10^6. The experimental transition point was specified as the 43.5%-chord point. The calculated and the experimental (flight) values are 2.32×10^{-3} and 2.30×10^{-3}, respectively. It is interesting to note that when the drag of the same airfoil was calculated in reference 4, the same drag coefficient, as the one computed in the present study, was obtained.

Figure 19 shows a comparison of calculated and experimental results for the NACA 63_3-018 airfoil [27,32]. For this airfoil the experimental pressure distributions were given for $R_c = 5.8 \times 10^6$ at angles of attack of $\alpha = 0 - 10$ in the unstalled regime. In the calculations, the transition points

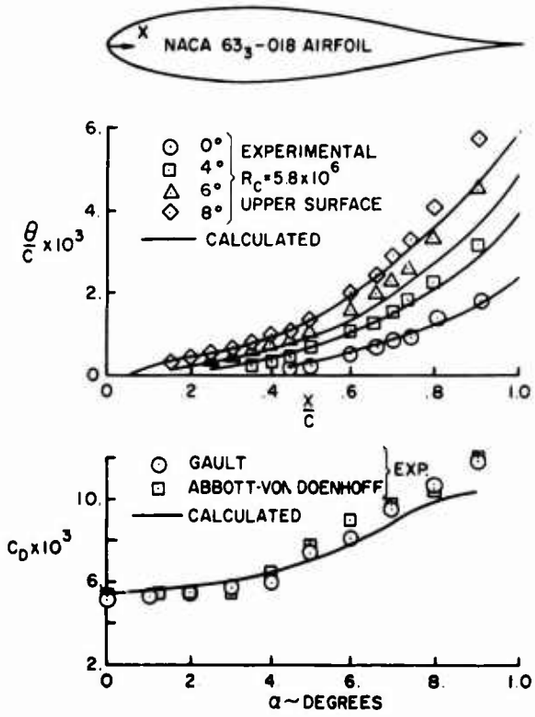

Figure 19. Calculated and experimental results for the NACA 63_3-018 airfoil [32]. Transition points were calculated by Michel's method.

were calculated by Michel's method since the experimental points were not given. In addition, the velocity distribution was extrapolated linearly from the 95%-chord point to the trailing edge since the experimental velocity distribution was given only to the 95%-chord point.

Finally, we present the results for the symmetrical NACA four-digit airfoils with thicknesses from 6 to 12% for zero angle of attack. Except for the 12%-thick airfoil the calculations were made by using the inviscid pressure distribution given in [27]. Again, the velocity distributions were extrapolated linearly from 95%-chord point to the trailing edge. The calculations for 0006 and 0009 airfoils were made for chord Reynolds number of 6×10^6. For the 0012 airfoil calculations were made for chord Reynolds numbers of 6×10^6 and 10.25×10^6 for the experimental distribution given in [33]. In these calculations the transition points were calculated by Michel's method. A comparison of the calculated and experimental drag coefficients for these airfoils is given in Table 2.

Table 2

A COMPARISON OF CALCULATED AND EXPERIMENTAL DRAG COEFFICIENTS FOR THE NACA 00-SERIES

Transition Positions were Calculated by Michel's Method

Airfoil	$R_c \times 10^{-6}$	$C_{D_{exp}} \times 10^3$	$C_{D_{cal}} \times 10^3$
0006	6	5.00	5.10
0009	6	5.50	5.52
0012	6	5.70	5.62
0012	10.25	5.60	5.30

We have also calculated the drag coefficients of several airfoils by using Granville's method for predicting the position of transition. It is important to note that when we calculate the boundary-layer parameters around the airfoil (one surface) we use about thirty chord stations. This means that each chord station is approximately three to four-percent-chord apart (in some cases, a little more). In calculating the transition point we first calculate the R_θ at each chord station and check whether the value at that station, defined by a certain R_x, satisfies the R_θ, R_x relationship of Michel. In following this procedure, a three- to four-percent error is introduced into the transition calculations. Such an error can, of course, be eliminated if one introduces more chordwise stations (which means longer computation times), or if a search is made for the transition point by extrapolating the calculated R_θ-values from one station to another. In using Granville's method, the error may double since this time it is necessary to search for the R_{θ_i}-value as well as for the $R_{\theta_{tr}}$-value. This means that it is necessary to introduce additional interpolation schemes into the numerical method if the transition is to be predicted accurately.

At the writing of this report, drag calculations using Granville's method are not finished. Because of the time available in the present study, we have not been able to introduce the proper procedure of calculating transition into the numerical method. For this reason, preliminary results will be presented only for three airfoils.

Figure 20 shows a comparison of calculated and experimental drag coefficients for the NACA 4412 airfoil for which the drag coefficients were obtained earlier by using Michel's method. The results indicate better agreement with experiment when the transition points are calculated by Granville's method. Table 3 presents a comparison of calculated transition points by each method as well as a comparison of calculated and experimental drag coefficients.

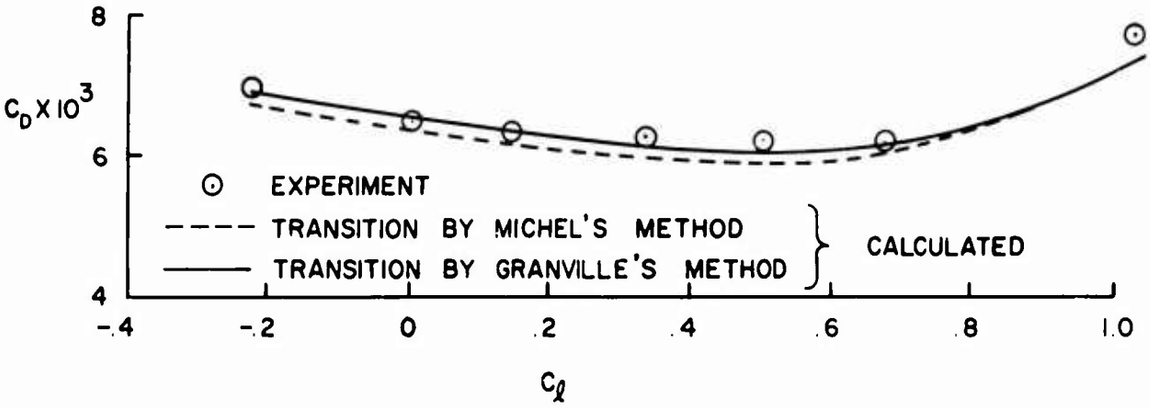

Figure 20. Comparison of calculated and experimental drag coefficients for the NACA 4412 airfoil at $R_c = 6 \times 10^6$. The calculated drag coefficients were obtained by using Michel's and Granville's methods.

Table 3

COMPARISON OF CALCULATED TRANSITION POINTS AND DRAG COEFFICIENTS FOR THE NACA 4412 AIRFOIL AT $R_c = 6 \times 10^6$

Angle of Attack α	Calculated Transition Points				Drag Coefficients $C_D \times 10^3$		
	Michel		Granville		Calculated		
	$\left(\frac{x}{c}\right)_u$	$\left(\frac{x}{c}\right)_\ell$	$\left(\frac{x}{c}\right)_u$	$\left(\frac{x}{c}\right)_\ell$	Transition by Michel	Transition by Granville	Experimental
-6	0.70	0.03*	0.65	0.03*	6.69	6.86	6.90
-4	0.65	0.03*	0.574	0.03*	6.31	6.52	6.45
-2	0.574	0.07*	0.50	0.07*	6.11	6.31	6.30
0	0.500	0.15	0.475	0.25*	5.83	5.49	6.25
2	0.45	0.25	0.40	0.225	5.79	6.01	6.20
4	0.35	0.52	0.325	0.400	5.96	6.04	6.20
8	0.126	1.00	0.126	1.00	7.27	7.27	7.60

*laminar separation

Calculations were also made for the NACA 35-215 and $65_{(215)}$-114 airfoils. For the first airfoil the calculated transition point by Granville's method agreed exactly with the one calculated by Michel's method and with the one obtained experimentally $[(x/c)_{tr} = 0.435]$. On the other hand, the transition points for the NACA $65_{(215)}$-114 changed slightly from those predicted by Michel's method. The difference in transition points affected the calculated drag coefficients as shown in Table 4.

Table 4

COMPARISON OF CALCULATED AND EXPERIMENTAL TRANSITION POINTS AND DRAG COEFFICIENTS FOR THE NACA $65_{(215)}$-114 AIRFOIL AT $C_\ell = 0.14$ [25]

$R_c \times 10^{-6}$	Calculated Transition Points				Experimental Transition Points		Drag Coefficients $C_D \times 10^3$		
	Michel		Granville				Calculated		
	$\left(\frac{x}{c}\right)_u$	$\left(\frac{x}{c}\right)_\ell$	$\left(\frac{x}{c}\right)_u$	$\left(\frac{x}{c}\right)_\ell$	$\left(\frac{x}{c}\right)_u$	$\left(\frac{x}{c}\right)_\ell$	Transition by Michel	Transition by Granville	Experimental
6	0.55	0.575*	0.525	0.55	0.567	0.562	4.22	4.54	4.40
8	0.525	0.55	0.5	0.525	0.562	0.555	4.12	4.46	4.26
10	0.525	0.525	0.5	0.525	0.558	0.552	4.03	4.23	4.10
15	0.50	0.50	0.475	0.50	0.534	0.532	3.97	4.10	4.00
20	0.45	0.50	0.45	0.475	0.483	0.507	3.99	4.05	4.10
30	0.35	0.40	0.39	0.425	0.391	0.447	4.38	4.16	4.40
40	0.30	0.325	0.35	0.40	0.334	0.372	4.63	4.27	4.80

*laminar separation

We note that the calculated drag coefficients in which the transition points are predicted by Granville's method are in better agreement with experiment than those obtained by Michel's method at lower Reynolds numbers. On the other hand, the trend is reversed at higher Reynolds numbers, the calculated values using Michel's method are in better agreement with experiment than those using Granville's

method. The discrepancy, however, can be also due to the inaccuracy of the procedure used to predict transition by Granville's method. Before a definite conclusion can be reached, it is necessary to improve the transition prediction procedures discussed before.

7.2 DRAG COEFFICIENTS OF AXISYMMETRIC BODIES

The total drag coefficient of an axisymmetric body can be calculated by using Young's formula [8]

$$C_D = \frac{2\theta_A}{A}\left(\frac{u_e}{u_\infty}\right)^{(h+5)/2} \tag{7.7}$$

where θ_A is the momentum area given by

$$\theta_A = 2\pi \int_0^\infty r \frac{u}{u_e}\left(1 - \frac{u}{u_e}\right)dy \tag{7.8}$$

and h is a shape factor defined as the ratio of displacement area δ_A^* to the momentum area θ_A. The former is given by

$$\delta_A^* = 2\pi \int_0^\infty r\left(1 - \frac{u}{u_e}\right)dy \tag{7.9}$$

In (7.7) A is the frontal area based on the maximum radius R_0 of the body,

$$A = \pi R_0^2 \tag{7.10}$$

and throughout this report it is used to normalize the drag coefficients. As in Squire-Young formula, the quantities θ_A, u_e/u_∞ and h in (7.7) are all to be evaluated at the tail end of the body.

A formula similar to Young's formula which can also be used to calculate the total drag coefficient of an axisymmetric body is Granville's formula [5].

$$C_D = \frac{2\theta_A}{A}\left(\frac{u_e}{u_\infty}\right)^{[(h+2)q+3]/q+1} \tag{7.11}$$

where q is a constant equal to 7. The difference between the two formulas (7.7) and (7.11) lies in the exponent of the u_e/u_∞ term.

In the case of axisymmetric bodies with large $r_o (r_o >> \delta)$, the momentum area θ_A becomes

$$\theta_a = 2\pi r_o \theta_{2-d} \tag{7.12}$$

In such cases, the shape factor reduces to its two-dimensional definition, $H = \delta^*/\theta$. Then (7.7) and (7.11) become

$$C_D = \frac{4r_o\theta_{2-d}}{R_o^2}\left(\frac{u_e}{u_\infty}\right)^{(H+5)/2} \tag{7.13}$$

and

$$C_D = \frac{4r_o\theta_{2-d}}{R_o^2}\left(\frac{u_e}{u_\infty}\right)^{[(H+2)7+3]/8} \tag{7.14}$$

A relation between (7.8) and (7.12) can be obtained by assuming a power law profile for the velocity profiles and by integrating (7.8) with this assumption. See reference 5. If we denote the two-dimensional definition of momentum area by θ_a and use the relations $u/u_e = (y/\delta)^{1/n}$, $r = r_o + y \cos\alpha$ in (7.8), we obtain

$$\frac{\theta_A}{\theta_a} = 1 + \frac{n+2}{2(2n+1)}\frac{\cos\alpha}{r_o/\delta} \tag{7.15}$$

Figure 21 shows the variation of θ_A/θ_a with r_o/δ for $n = 5$ and 10.

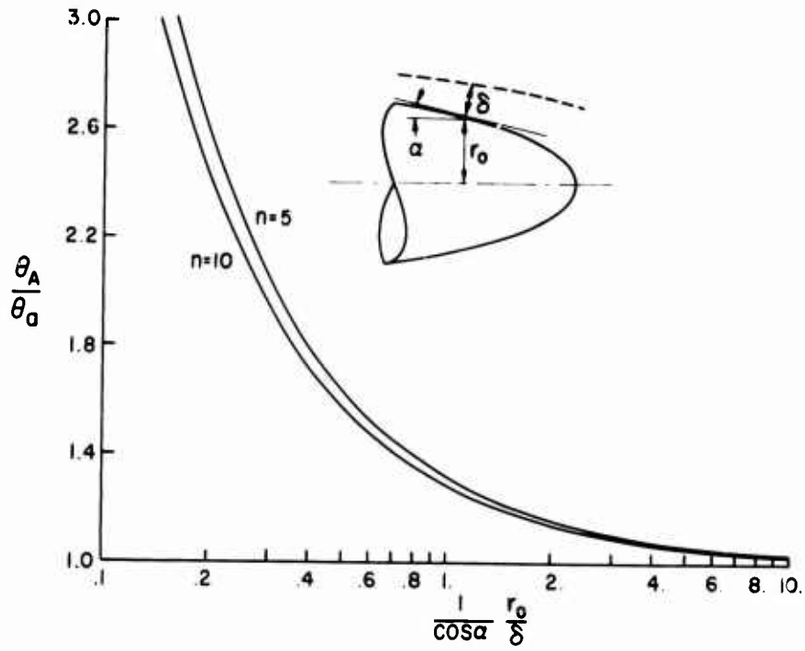

Figure 21. The variation of θ_A/θ_a with r_o/δ for two values of n.

The total skin-friction coefficient of an axisymmetric body, C_F, is obtained by integrating the local skin-friction coefficient c_f around the body. It is given by

$$C_F = \frac{2\pi}{A}\int_0^{x_{t.e.}} c_f r_o \left(\frac{u_e}{u_\infty}\right)^2 dx \tag{7.16}$$

where

$$c_f = \frac{\tau_w}{1/2\ \rho u_e^2} \tag{7.17}$$

In the study reported here, the total drag coefficients and total skin-friction coefficients of several axisymmetric bodies were calculated. We first present the results for some of the DTMB bodies measured by Gertler [34]. These bodies, which were all all 9-feet long, were tested in a water towing tank for a Reynolds number range of 2×10^6 to 26×10^6. The boundary layers were tripped at $x/L = 0.05$.

The drag calculations were performed for three bodies with fineness ratios of 4, 7, and 10. In the calculations we used the inviscid pressure distribution obtained from the Douglas Neumann method [2] because the experimental values were not given. However, in the case of the body with the fineness ratio of 4, viscous corrections were made to the inviscid pressure distribution (see Section 6.1). Figure 22 shows a comparison of two pressure distributions for this body. The results show that viscous effects have negligible effect on the pressure distribution up to 86%-chord point which corresponds to zero Cp.

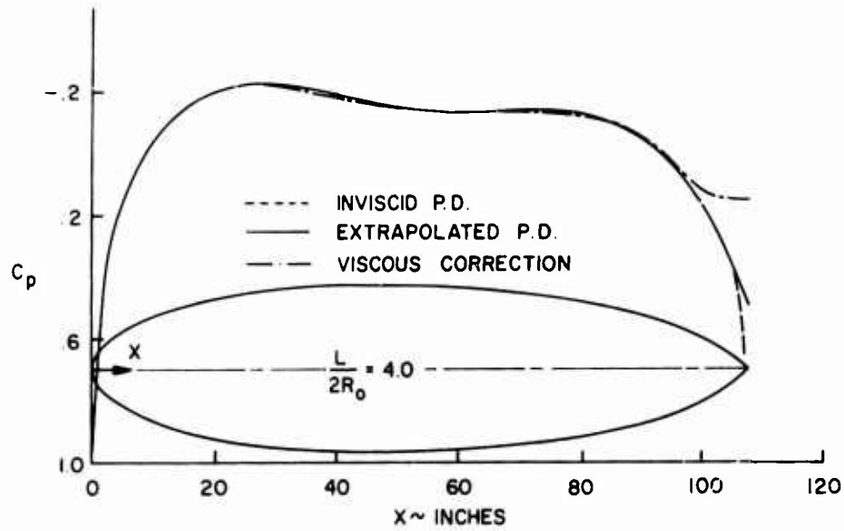

Figure 22. Pressure distribution on DTMB body 4154 with and without viscous correction $R_L = 4 \times 10^6$.

Between 86% chord-point and the tail end of the body, however, the pressure distribution with the viscous correction significantly changes from the inviscid pressure distribution. The calculated drag coefficients using the pressure distribution with and without the viscous effects at several chord points also vary significantly. Figure 23 shows the calculated total drag coefficients at several axial locations for the two pressure distributions. For the inviscid pressure distribution the drag calculations were only performed up to 89% chord point since flow separation was observed past this point. However, for the pressure distribution with the viscous corrections, no flow separation was observed, and the calculations were continued up to the tail end of the body. The results in figure 23 indicate that the drag formulas show great sensitivity

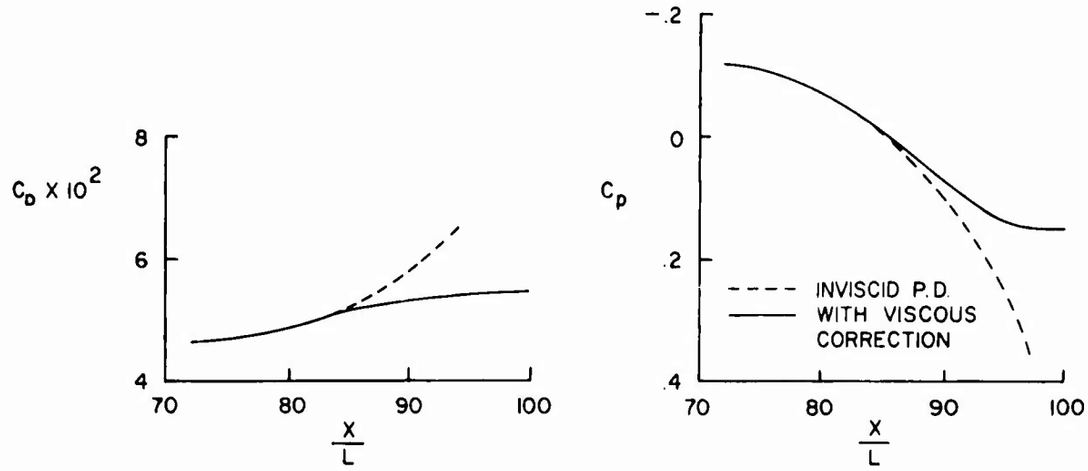

Figure 23. Variation of total drag coefficient with axial distance for the DTMB body 4154 at $R_L = 4 \times 10^6$ [34]. The total drag coefficient was calculated by using Granville's formula (7.14).

to the choice of tail end when inviscid pressure distribution is used. On the other hand, the sensitivity to the choice of the tail end disappears when the calculations are made by using the pressure distribution with viscous corrections. The results also indicate that the calculated drag values obtained by either (7.7) or (7.11) differ significantly from the experimental value. However, when the calculations are made by using (7.13) and (7.14), that is, by using equations that employ the two-dimensional definition of momentum area, θ_a, a better agreement is obtained with experiment. It is interesting to note that when the inviscid pressure distribution is used, the chord-point where $C_p = 0$ seems to give drag values which agree satisfactorily with experiment, at least for this body. At this point the wake correction term in the drag formula makes no difference because $u_e/u_\infty = 1.0$.

Figure 24 shows a comparison of calculated and experimental drag coefficients for the same body. The experimental values are not corrected for wave making resistance of the body. In this case, the calculations were made by using the inviscid pressure distribution. However, the calculated total drag coefficients were obtained by taking the tail end to be the point where $C_p = 0$. This is a reasonable approximation for this body since the inviscid pressure distribution does not deviate from the actual pressure distribution up to this chord point. In these calculations we have used the two-dimensional definition of momentum area. In this case, the total drag coefficient is given by

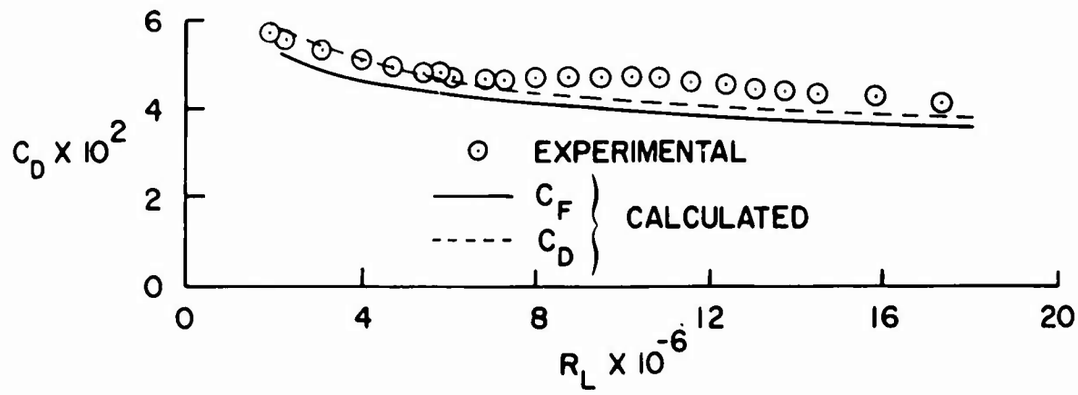

Figure 24. Comparison of calculated and experimental drag values for the DTMB body 4154 [34]. The total drag coefficients were obtained by using Granville's formula (7.14) and by taking the point where $C_p = 0$ as the tail end.

$$C_D = \frac{4r_o\theta_{2-d}}{R_o^2} \tag{7.18}$$

The calculated total drag values deviate a little from the experimental values. They can probably be improved if one obtains a viscous correction to the inviscid pressure distribution at each Reynolds number and then calculates the drag at the tail end of the body. However, this is not done in this study.

Figure 24 also shows the total skin-friction drag coefficient for this body. Calculations were made by using the inviscid pressure distribution in which the velocity distribution from the 95% chord point was extrapolated linearly to the tail end.

Figures 25 and 26 show the results for the bodies with fineness ratio of 7 and 10, respectively. In these cases, the calculations were made by using the inviscid pressure distribution. The total drag coefficients were again computed by using (7.18) and the total skin-friction coefficients by using (7.16). The calculated total drag coefficients and total skin-friction coefficients agree well, indicating that the pressure drag is negligible. This is reasonable since both bodies are quite slender.

We next present the results for a 285-foot long airship [35] with a fineness ratio of 4.2. For this body the pressure distribution and boundary-layer measurements were made in flight at speeds from 35 to 70 miles per hour.

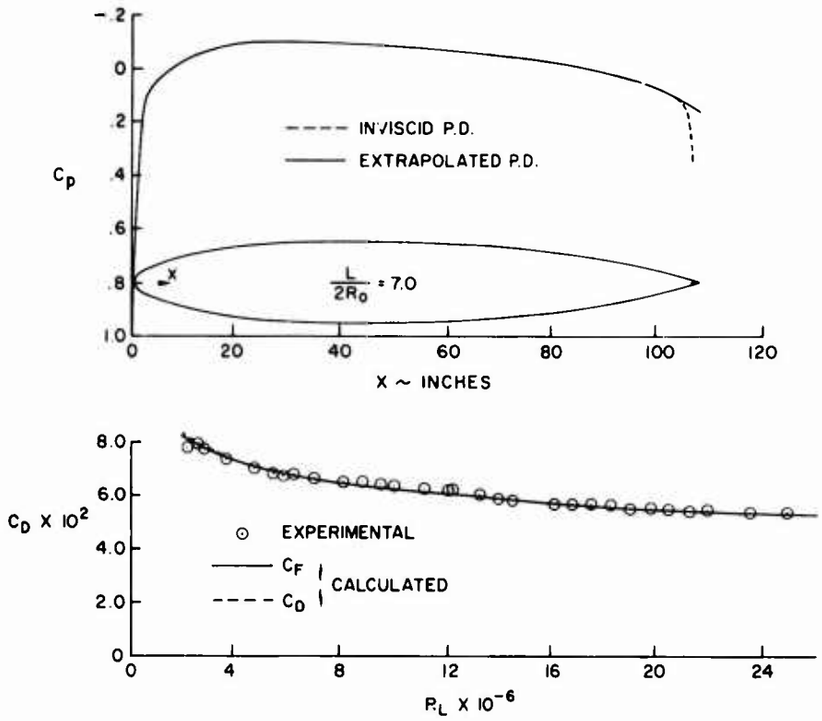

Figure 25. Comparison of calculated and experimental results for the DTMB body 4165 [34].

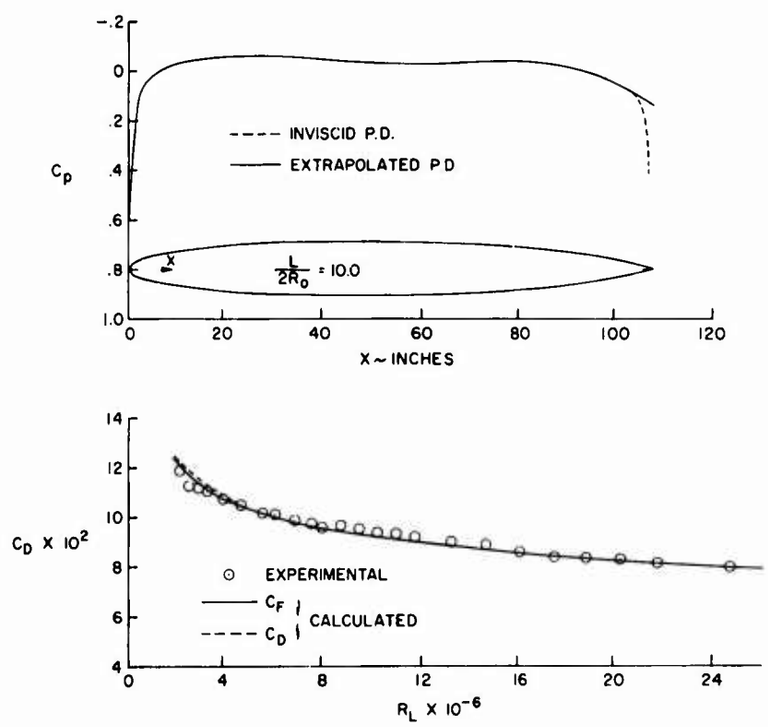

Figure 26. Comparison of calculated and experimental results for the DTMB body 4159 [34].

No transition data was given, but from the configuration of the airship it was implied that the boundary layer was tripped at approximately $x/L \approx 0.05$.

Calculations were made for the conditions corresponding to four different speeds for the airship envelope in its "original" configuration: u_∞ = 35, 50, 60 and 70 miles per hour corresponding to nominal length — Reynolds numbers, R_L, of 94, 135, 162 and 188 million.

Figures 27 and 28 show a comparison of calculated and experimental results for the airship. According to figure 27, the agreement in calculated and experimental δ^* and θ-values is very good at high Reynolds numbers.

The experimental total drag coefficients in figure 28 were obtained both from extrapolations of the velocity profiles at $x/L = 0.96$ into the wake and from the horsepower requirements of the airship envelope. The calculated total drag coefficients were obtained by using Granville's formula (7.14) and the calculated total skin-friction drag coefficients were obtained from (7.16). In applying Granville's formula, the total drag values were calculated at several chord points near the 96% chord point because the experimental pressure distribution was given up to the 96% chord point. The total drag of the body was obtained by extrapolating the results to the tail end.

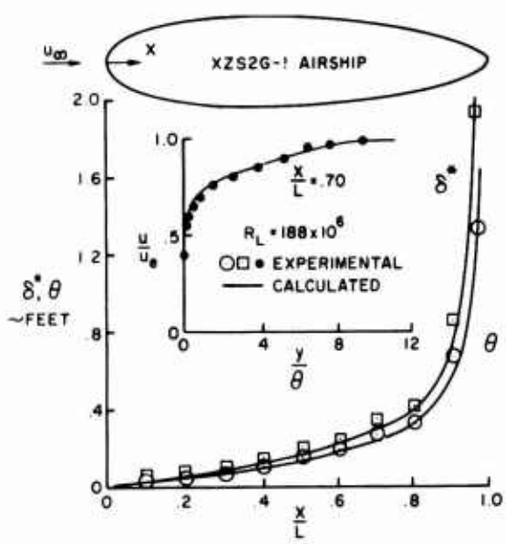

Figure 27. Comparison of calculated and experimental results for the XZS2G-1 airship at $R_L = 188 \times 10^6$ [35].

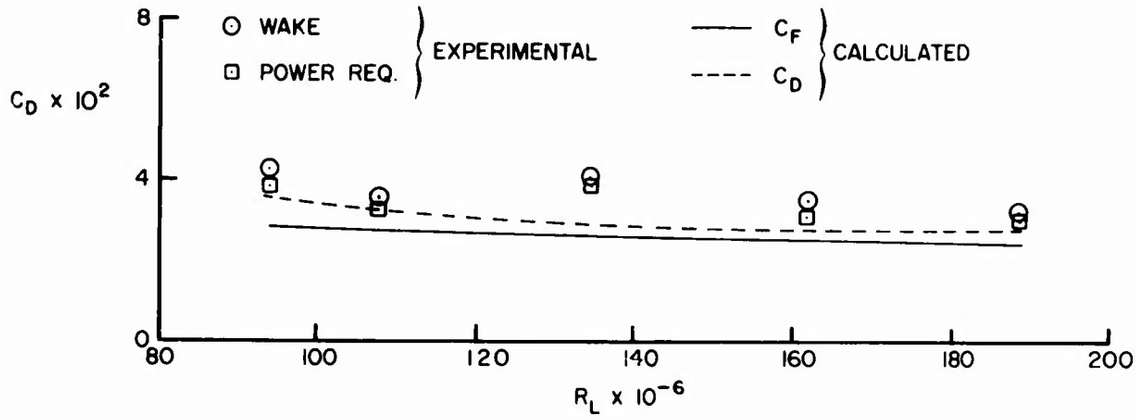

Figure 28. Comparison of calculated and experimental drag values for the XZS2G-1 airship [35]. Total drag coefficients were obtained by Granville's formula (7.14).

Finally we present the results for the boundary-layers measured by Murphy [36]. In this reference, Murphy presented quite detailed experimental data on bodies of revolution of different shapes. The experimental data included experimental pressure distributions, skin friction coefficients, velocity profiles and separation point locations.

The calculations were made for three different shapes which represented a combination of one basic nose shape (A-2), a constant area section, and different tail shapes (Tails A-2, C-2, and C-4). Transition was tripped at an axial location of 31 inches from the nose of the body by a two-inch wide porous strip, which was used for mass transfer measurements and was sealed for zero mass transfer. The skin friction coefficients were obtained by Preston tube, and experimental total drag coefficients were obtained from the wake profile.

Figure 29 shows a comparison of calculated and experimental c_f and R_θ-values. It is important to note that the agreement is quite good considering the fact that the calculations were started at the stagnation point and transition was specified at 31 inches. The calculated values in this manner match the experimental values and a little discrepancy in skin friction may be attributed to the effect of the porous strip.

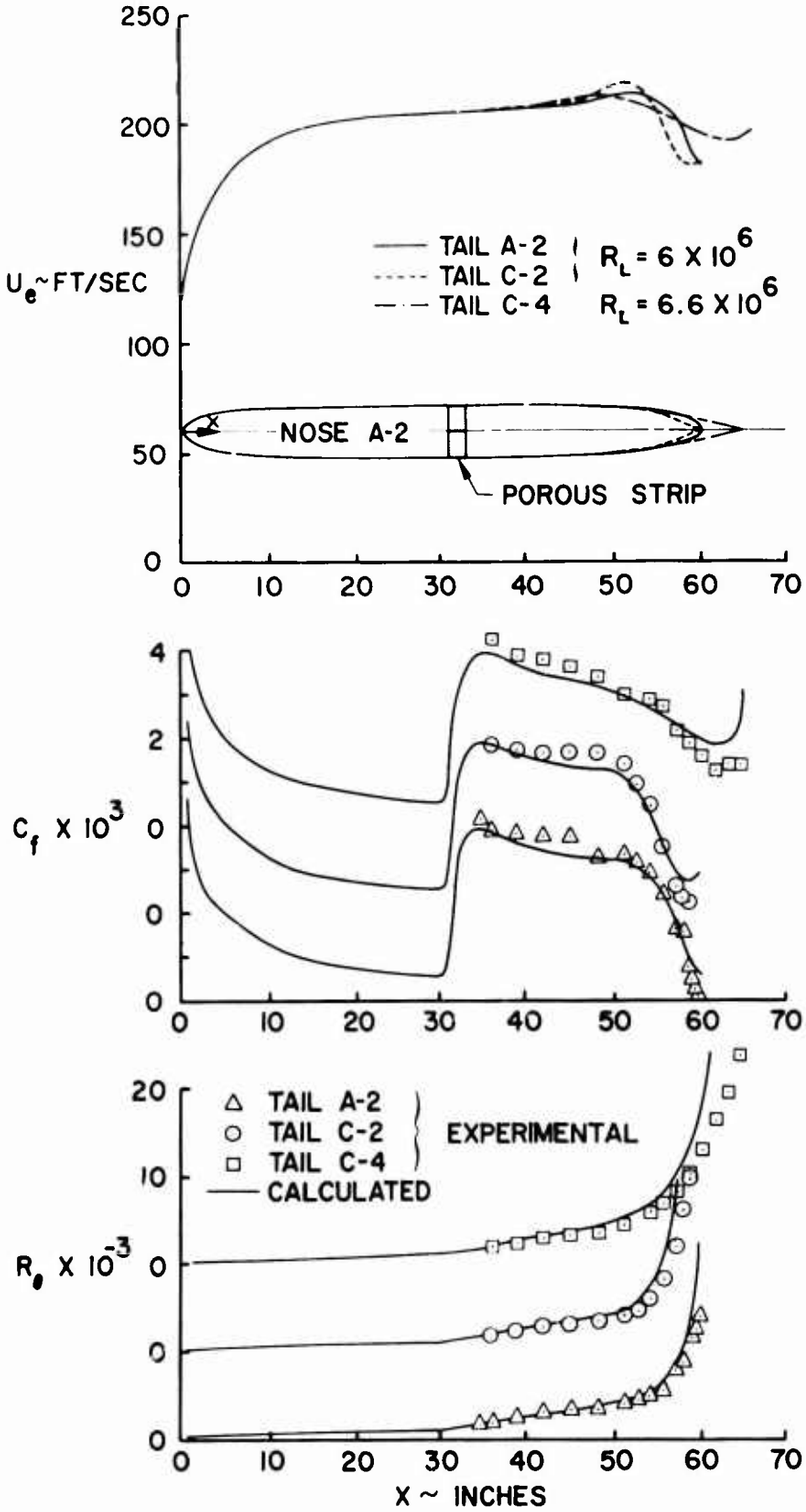

Figure 29. Comparison of calculated and experimental results for the Murphy bodies of revolution [36].

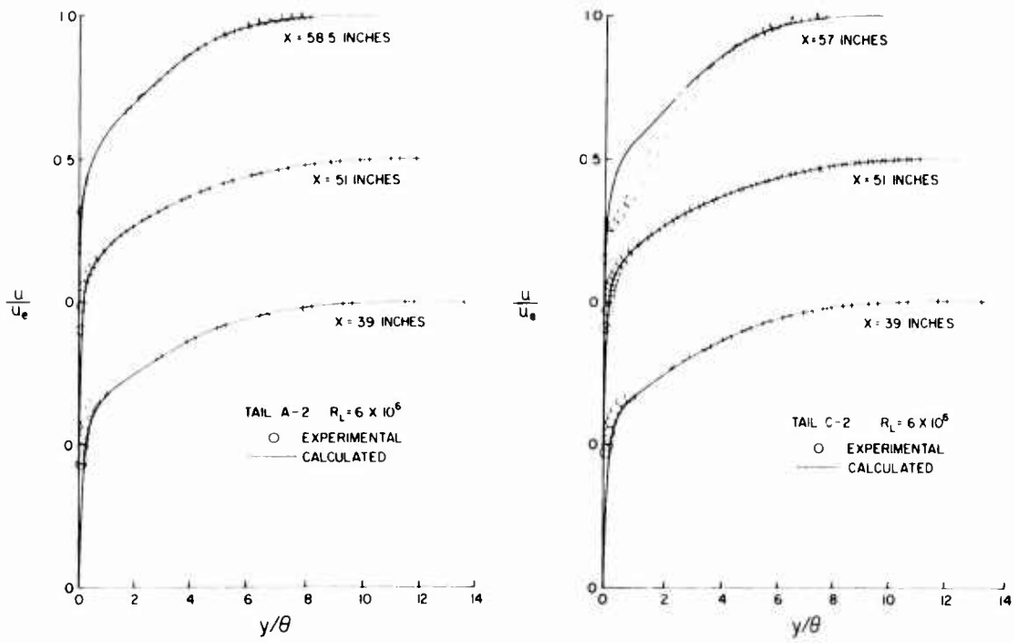

Figure 30. Comparison of calculated and experimental velocity profiles for the Murphy bodies of revolution [36].

Figure 30 shows a comparison of calculated and experimental velocity profiles for two tail shapes, namely, A-2 and C-2. Except for one station the results are in agreement with experiment. The discrepancy in the velocity profile of shape C-2 at $x = 57$ inches may be due to flow separation since separation in this case was reported at $x = 58.3$ inches.

Table 5 presents a comparison of calculated and experimental drag coefficients for the Murphy bodies. The calculated drag coefficients obtained by Granville's formula (7.14), include both total drag and total skin-friction coefficients. It is interesting to note that the experimental total drag coefficients which were obtained by the wake profile method agree well with the calculated total skin-friction coefficients and not with the calculated total drag coefficients. The nose pressure distributions of these bodies are not representative of those on a body located in an undisturbed stream because in the tests the nose of the body extended about 1.5 feet into the wind-tunnel contraction section. For this reason, it is possible that the calculated drag coefficients may give the correct total drag of these bodies.

Table 5

COMPARISON OF CALCULATED AND EXPERIMENTAL DRAG COEFFICIENTS FOR THE MURPHY BODIES [36]

Tail Shape	Experimental Total Drag	Calculated Total Drag	Calculated Total Skin-Friction
A-2	0.072 ± 0.003	0.075	0.072
C-2	0.071 ± 0.002	0.076	0.068
C-4	0.072 ± 0.002	0.075	0.069

8.0 CALCULATION OF TURBULENT BOUNDARY-LAYER SEPARATION ABOUT TWO-DIMENSIONAL AND AXISYMMETRIC BODIES IN INCOMPRESSIBLE FLOWS

8.1 METHODS FOR PREDICTING TURBULENT BOUNDARY-LAYER SEPARATION

In many problems it is necessary to know whether the boundary layer, either laminar or turbulent, will separate from the surface of a specific body, and if so, where the flow separation will occur. This is quite important since in many design problems, such as for example, in the design of hydrofoils or airfoils, it is necessary to prevent flow separation in order to reduce drag and to obtain high lift.

For steady flows, the separation point is defined as the point where the wall shear stress, τ_w, is equal to zero, that is,

$$\left(\frac{\partial u}{\partial y}\right)_w = 0$$

With high-speed computers, the governing boundary-layer equations for laminar flow can be solved exactly, and consequently the laminar separation point can be determined almost exactly. In addition, there are several "simple" methods which do not require the solution of the boundary-layer equations in their differential form and can be used to predict separation point quite satisfactorily. The momentum integral method of Thwaites and the method of Stratford are examples of two of such methods. The latter method does not even require the solution of the laminar boundary-layer equations. For a given pressure distribution, for example, $C_p(x)$, the expression

$$C_p^{1/2}\left(x\,\frac{dC_p}{dx}\right)$$

is calculated around the body. Separation is predicted when it reaches a value of 0.102.

The prediction of separation point in turbulent flows, on the other hand, is a much more difficult job. Due to the presence of the time mean of the

fluctuating quantities appearing in the governing equations, an exact solution of the boundary-layer equations for turbulent flows is impossible. Consequently, when the equations are solved with some suitable assumption for these quantities, the solutions contain empiricism and must be checked against experiment.

The current prediction methods on the subject can be divided into two groups. In one group we have methods that require the detailed solution of the boundary-layer equations. These methods are either of differential type (meaning that partial-differential equations are solved) or of integral type (meaning that momentum integral or energy integral equations are solved). Reference 20 presents a critical evaluation of these methods for two-dimensional incompressible turbulent flows. In differential methods the parameter used to predict the separation point is the zero wall shear stress. In integral methods, on the other hand, the shape factor $H = \delta^*/\theta$ is usually used to locate the separation point. In integral methods as the flow approaches separation, the value of H increases. Separation of the flow is assumed to occur when H reaches a value between 1.8 and 2.4. In some cases, however, the value of H increases rapidly near separation and then begins to decrease. In such cases*, the point corresponding to the maximum value of H is taken as the separation point.

In another group, we have methods that do not require the detailed boundary-layer calculations. Separation is predicted by simple formulas or by "simple" differential equations that are very fast and easy to apply. These methods also utilize the composite nature of the turbulent boundary layer. For example, Stratford [37] divides the turbulent boundary layer into inner and outer regions and bases his analysis on the assumptions that in the outer region the pressure forces cause a direct reduction in dynamic head and that in the inner region the pressure force is balanced by the shear-force gradient. Goldschmied's method also treats the boundary layer consisting of inner and outer regions. His analysis is based on the assumptions of inner-region similarity under any pressure gradient and of a constant total-head line at a fixed distance from the wall.

---

*These cases correspond to flows for which the calculations are made using an experimental pressure distribution.

In this report we study the accuracy of the several current methods for predicting the turbulent boundary-layer separation point. In particular, we consider a differential method (Douglas boundary-layer method), a momentum integral method (Head's method) and two "simple" methods, namely, the methods of Stratford [37] and Goldschmiedt [38]. These methods are briefly described below. Since the Douglas boundary-layer method has already been discussed in a previous section, the discussion is presented only for the other methods. Results obtained by these methods are described in Section 9.

8.1.1 Head's Method

Head's method is an integral method that can be used both for calculating the boundary-layer parameters as well as for predicting the position of separation in turbulent flows. It uses the momentum integral equation

$$\frac{d\theta}{dx} + (H + 2)\frac{\theta}{u_e}\frac{du_e}{dx} = \frac{c_f}{2} \tag{8.1}$$

and two auxiliary equations, namely, Ludwieg-Tillman's expression for the skin-friction coefficient,

$$c_f = 0.246(10)^{-0.678H}R_\theta^{-0.268} \tag{8.2}$$

and a shape factor G(H) relationship obtained from the entrainment properties of the turbulent boundary layer. The latter is also related to another shape factor H_1. The entrainment and the shape factor relationships are as follows:

<u>Entrainment relation</u>

$$\frac{1}{u_e}\frac{d}{dx}(u_e\theta H_1) = 0.0299(H_1 - 3.0)^{-0.6169} \tag{8.3}$$

<u>Shape Factor relation</u>

$$H_1 = G(H)$$

where

$$G(H) \begin{cases} 0.8234(H - 1.1)^{-1.287} & H \leq 1.6 \\ 1.5501(H - 0.6778)^{-3.064} + 3.3 & H \geq 1.6 \end{cases} \tag{8.4}$$

This method like most integral methods, uses the shape factor H as the criterion for separation. Although it is not possible to give an exact value of H corresponding to separation, when H is between 1.8 and 2.4, separation is assumed to exist. The difference between the lower and upper limits of H makes very little difference in locating the separation point, since close to separation the shape factor quickly increases.

The momentum integral equation (8.1) has within it the assumption that the Reynolds normal stresses can be neglected, a fact that has been disputed by a number of authors. The validity of this assumption has been questioned, for example, see reference 39. With the normal-stress terms, the momentum integral equation is

$$\frac{d\theta}{dx} + (H + 2)\frac{\theta}{u_e}\frac{du_e}{dx} = \frac{c_f}{2} + \frac{\partial}{\partial x}\int_0^\infty (\overline{u'^2} - \overline{v'^2})dy \tag{8.5}$$

The term $\overline{u'^2}$ comes directly from the x-momentum equation. The $\overline{v'^2}$ term enters the equation because of static-pressure variation across the boundary layer.

In reference 40 calculations were made to investigate the importance of the Reynolds normal stresses. It was found that in general

$$\int_0^\infty \frac{\partial}{\partial x}\overline{v'^2}\, dy = \frac{1}{2}\int_0^\infty \frac{\partial}{\partial x}\overline{u'^2}\, dy$$

Based upon this approximation, the following formula was obtained for the normal-stress correction (NSC)

$$NSC = 0.0365(H - 1)\frac{d\delta^*}{dx} \tag{8.6}$$

This correction depends on the derivative of δ^* and leads to a singularity in the momentum integral equation. When H is approximately 5.7, $d\theta/dx$ becomes infinite. However, the singularity should not be a practical limitation, since separation occurs for values of H well below 5.7.

In the study reported here we have added the NSC term to Head's method and have compared the results with those obtained without this correction for several test cases. Although in some cases the addition of NSC-term improved the results, the improvement was not significant. Consequently, addition of the NSC-term to Head's method was omitted in the present study.

8.1.2 Stratford's Method

Stratford's method for turbulent flows is a simple method that uses only the pressure distribution to predict boundary-layer separation. It does not require the detailed boundary-layer calculations like the Douglas boundary-layer method or Head's method. Presently there are several methods based on the ideas set forth in this method [41,42]. However, the accuracy of these methods is similar to Stratford's method and are not considered in detail in this report.

Stratford's method is based upon the ideas of dividing the boundary layer into outer and inner portions. It follows the principles successfully adopted for laminar flow. Briefly, the method can be described as follows.

Consider a flow in which the pressure is constant between $0 \leq x \leq x_0$ and a fairly sharp pressure rise from $x > x_0$. The boundary layer is divided into outer and inner portions. In the outer portion the flow is nearly inviscid so that we can write Bernoulli's equation as

$$p + \frac{1}{2}\rho u^2(x,\psi) = p_0 + \frac{1}{2}\rho u^2(x_0,\psi) + \Delta H_1 \tag{8.7}$$

where the stream function ψ is given by

$$\psi = \int_0^y u\, dy \tag{8.8}$$

and ΔH_1 denotes a (small) correction for the effects of viscosity.

For a constant pressure flow $(p = p_o)$, which Stratford calls the "comparison" flow, the loss of total head ΔH_2 is

$$\Delta H_2 = \frac{1}{2}\rho u_c^2(x,\psi) - \frac{1}{2}\rho u_c^2(x_o,\psi) \tag{8.9}$$

If we now assume that $\Delta H_1 = \Delta H_2$ and substitute (8.9) into (8.7), we obtain

$$\frac{1}{2}\rho u^2(x,\psi) = \frac{1}{2}\rho u_c^2(x,\psi) - (p - p_o) \tag{8.10}$$

since $u = u_c$ for $x \leq x_o$.

Differentiating (8.10) with respect to ψ, yields

$$u\left(\frac{\partial u}{\partial y}\right)\left(\frac{\partial y}{\partial \psi}\right) = u_c\left(\frac{\partial u_c}{\partial y_c}\right)\left(\frac{\partial y_c}{\partial \psi}\right)$$

or

$$\frac{\partial u}{\partial y} = \frac{\partial u_c}{\partial y_c} \tag{8.11}$$

Assumption of a power-law profile for the "comparison" velocity profile, that is,

$$\frac{u_c}{u_o} = \left(\frac{y_c}{\delta}\right)^{1/n} \tag{8.12}$$

and use of (8.8) and (8.11) yields the following expressions for the outer portion of the boundary layer:

$$\frac{\partial u_c}{\partial y_c} = \frac{u_o}{\delta n}\left(\frac{y_c}{\delta}\right)^{(1/n)-1} \tag{8.13}$$

$$u_c = u_o \left(\frac{y_c}{\delta}\right)^{1/n} \tag{8.14}$$

$$\psi_c = \frac{n u_o \delta}{n+1} \left(\frac{y_c}{\delta}\right)^{(n+1)/n} \tag{8.15}$$

In the inner portion of the boundary layer close to the wall, since u and v are small, the momentum equation can be written as

$$\frac{\partial \tau}{\partial y} = \frac{dp}{dx} \tag{8.16}$$

Integrating the above expression, we get

$$\tau = \tau_w + \frac{dp}{dx} y \tag{8.17}$$

At separation $\tau_w = 0$. Equation (8.17) then becomes

$$\tau = \frac{dp}{dx} y \tag{8.18}$$

We now represent the shear stress τ by Prandtl's mixing-length expression $\tau = \rho(ky)^2(du/dy)^2$ and write (8.18) as

$$\frac{du}{dy} = \left(\frac{1}{k^2} \frac{1}{\rho y} \frac{dp}{dx}\right)^{1/2} \tag{8.19}$$

Successive integration of (8.19) gives

$$u = \left(\frac{4}{k^2} \frac{dp}{dx} \frac{y}{\rho}\right)^{1/2} \tag{8.20}$$

$$\psi = \frac{4}{3}\left(\frac{1}{\rho k^2} \frac{dp}{dx}\right)^{1/2} y^{3/2} \tag{8.21}$$

We next use the appropriate joining conditions, namely, continuity of τ, u, and $\partial u/\partial y$ and obtain

$$C_p^{n-2}\left(x\frac{dC_p}{dx}\right)^2 = 3(n-2)^{n-2}(n+1)^{-n+1}\,k^4 n^{-2}\left(\frac{\delta_c}{x}\right)^{-2} \tag{8.22}$$

where

$$C_p = \frac{p-p_o}{1/2\,\rho u_o^2} = 1 - \frac{u_e^2}{u_o^2} \tag{8.23}$$

If we assume that the "comparison" boundary-layer thickness is given by

$$\frac{\delta_c}{x} = 0.37\,R_x^{-1/5} \tag{8.24}$$

then substitution of (8.24) into (8.22) with $n = 6$ gives

$$C_p\left(x\frac{dC_p}{dx}\right)^{1/2} = \frac{(0.64)k}{2}\,R_x^{1/10}$$

or

$$\left(\frac{2.5}{0.64}\right)C_p\left(x\frac{dC_p}{dx}\right)^{1/2} R_x^{-1/10} = \frac{2.5}{2}\,k$$

or since $(2.5/0.64) = 10^{0.6}$

$$C_p\left(x\frac{dC_p}{dx}\right)^{1/2}\left(10^{-6}R_x\right)^{-1/10} = \frac{2.5}{2}\,k \equiv F(x) \tag{8.25}$$

The above analysis assumes an adverse pressure gradient starting from the leading edge as well as fully turbulent flow everywhere. When there is a region of laminar flow, or a region of turbulent flow with a favorable pressure gradient, Stratford makes the assumption that at the minimum pressure point, $x = x_m$, the velocity profile is approximately that of a flat-plate turbulent boundary layer starting from a false origin $x = x'$. Thus we replace x by $(x - x')$ in (8.25) and take the value of R_x as $u_m(x - x')/\nu$. We determine the appropriate x' as follows.

In the initial region of laminar flow the momentum thickness can be calculated by Thwaites' method, that is,

$$\theta = \left(0.45\nu u_e^{-6} \int_0^x u_e^5 \, dx\right)^{1/2} \tag{8.26}$$

so that at the transition point,

$$\theta_{tr} = \left[0.45 \frac{\nu}{u_{tr}} \int_0^{x_{tr}} \left(\frac{u_e}{u_{tr}}\right)^5 dx\right]^{1/2} \tag{8.27}$$

Downstream of transition we calculate the momentum thickness for turbulent flows by the expression given in reference 24,

$$\left(\theta R_\theta^{1/5} u_e^4\right)_{x_{tr}}^{x} = 0.0106 \int_{x_{tr}}^{x} u_e^4 \, dx \tag{8.28}$$

where $R_\theta = u_e\theta/\nu$. At the minimum pressure point, $x = x_m$, (8.28) becomes

$$\theta_m R_{\theta_m}^{1/5} = 0.0106 \int_{x_{tr}}^{x_m} \left(\frac{u_e}{u_m}\right)^4 dx + \theta_{tr} R_{\theta_{tr}}^{1/5} \left(\frac{u_{e_{tr}}}{u_m}\right)^4 \tag{8.29}$$

If we now assume that θ is continuous at transition, then we can substitute (8.27) into (8.29) and obtain

$$\theta_m R_{\theta_m}^{1/5} = 0.0106 \int_{x_{tr}}^{x_m} \left(\frac{u_e}{u_m}\right)^4 dx + \frac{\nu}{u_m} \left[0.45 \frac{u_{tr}}{\nu} \int_0^{x_{tr}} \left(\frac{u_e}{u_m}\right)^5 dx\right]^{3/5} \tag{8.30}$$

But for a flat-plate turbulent boundary layer the value of θ at a distance $(x_m - x')$ from the leading edge, with $u_e = u_m$ according to (8.28) is

$$\theta_m R_{\theta_m}^{1/5} = 0.0106 \, (x_m - x') \tag{8.31}$$

By equating (8.30) and (8.31) we obtain the result

$$x_m - x' = 58 \frac{\nu}{u_m} \left[\frac{u_{tr}}{\nu} \int_0^{x_{tr}} \left(\frac{u_e}{u_m} \right)^5 dx \right]^{3/5} + \int_{x_{tr}}^{x_m} \left(\frac{u_e}{u_m} \right)^4 dx \qquad (8.32)$$

With the expression given by (8.32), equation (8.25) can be used to predict the separation point in turbulent flows. In order to do this, however, it is necessary to assume a value for k, which according to the mixing length theory, is 0.4. This means that the right-hand side of (8.25) should be of order 0.5, but a comparison with experiment, according to Stratford, suggests a smaller value of $F(x)$ around 0.35 and 0.40. For a typical turbulent boundary-layer flow with an adverse pressure gradient, it is found that $F(x)$ increases as separation is approached and decreases after separation. For this reason, after applying his method to several flows with turbulent separation, Stratford observed that if the maximum value of $F(x)$

a. is greater than 0.40, separation is predicted when $F(x) = 0.40$;

b. lies between 0.35 and 0.40, separation recurs at the maximum value;

c. is less than 0.35, then separation does not occur.

8.1.3 Goldschmied's Method

Goldschmied's separation criterion [38], like Stratford's method, is based on the existence of inner and outer regions in the turbulent boundary layer. Goldschmied assumes that there is a line in the inner region at a constant distance y_c from the wall with constant total head, h_c, such that

$$h_c = p + \frac{1}{2} \rho u_c^2 \qquad (8.33)$$

Furthermore, since the line is in a region where the law of the wall applies, he assumes it to be independent of pressure distribution and selects the outer edge of the inner region at the start of the adverse pressure gradient as the starting point of the line. He assumes that the outer edge of the inner region is characterized approximately by $u/u^* = 20$ and $yu^*/\nu = 500$. Then the total head at the start of adverse pressure gradient can be written as

$$h_o = p_o + \frac{1}{2}\rho(20u_m^*)^2 \tag{8.34}$$

Then from (8.33) and (8.34),

$$p_o - p + \frac{1}{2}\rho 400 \frac{\tau_w}{\rho} = \frac{1}{2}\rho u_c^2 \tag{8.35}$$

since $u_m^* = \sqrt{\tau_w/\rho}$. Dividing both sides of (8.35) by u_m^2 and rearranging gives

$$\left(\frac{u_c}{u_m}\right)^2 = \frac{p_o - p}{1/2\ \rho u_m^2} + 400\ \frac{\tau_w}{\rho u_m^2} \tag{8.36}$$

If the following terms are defined,

$$c_{f_m} \equiv \frac{\tau_w}{1/2\rho u_m^2} \qquad \text{and} \qquad C_p \equiv \frac{p - p_o}{1/2\ \rho u_m^2}$$

Equation (8.36) becomes

$$\frac{u_c}{u_m} = (200c_{f_m} - C_p)^{1/2} \tag{8.37}$$

Making use of the laminar sublayer and the law of the wall, he further shows that at separation the expression $u_c/u_m = 1/3.45\ [c_{fm}/2]^{1/2}$ is so small that it can be neglected. Then (8.37) reduces to

$$C_{p_s} = 200\ c_{f_m} \tag{8.38}$$

and becomes the separation criterion for Goldschmied's method.

9.0 COMPARISON OF CALCULATED AND EXPERIMENTAL TURBULENT BOUNDARY-LAYER SEPARATION IN TWO-DIMENSIONAL AND AXISYMMETRIC FLOWS

In this section we consider several experimental pressure distributions which include observed or measured boundary-layer separation, and apply the four separation-prediction methods discussed in Section 8 to these pressure distributions. It is important to note that near separation the behavior of these methods with an experimental pressure distribution is quite different from that with an inviscid pressure distribution. The pressure distribution near the point of separation may be a characteristic of the phenomenon of separation and inclusion of it in the specification of the flow is equivalent to being told the position of separation [41]. For this reason, use of these separation-prediction methods with an experimental pressure distribution will only show their behavior close to separation and indicate whether the theoretical assumptions used in these methods are self-consistent. When one considers an experimental pressure distribution with separation and uses the Douglas boundary-layer method, it is quite possible that the wall shear stress at the experimental separation point may not approach zero. It may decrease as the separation is approached and may start to increase past the separation point. Similarly, the shape factor H in Head's method may not show a continuous increase to the position of separation. Depending on the pressure distribution which is distorted by the separation flow, the shape factor may even start to decrease after an increase. All that can be learned from a study such as the one conducted here is how these methods behave close to separation, and whether they predict an early separation or no separation at all.

In the study reported here, we have tested these methods for a number of two-dimensional and axisymmetric flows with separation. During the study it became necessary to make certain assumptions in applying Goldschmied's method. According to this method it is necessary to calculate the local turbulent skin-friction coefficient at the minimum pressure point. In the cases studied here, however, the flow is generally laminar at the minimum pressure point and becomes turbulent downstream of that point. In these cases, the calculated local skin-friction coefficient for turbulent flow was extrapolated to the minimum pressure point.

It was also observed that Stratford's method gave better agreement with experiment provided that the range of $F(x)$ was slightly changed from that given in Section 8.1.2, namely if the maximum value of $F(x)$: (a) is greater than 0.50, separation is predicted when $F(x) = 0.50$; (b) lies between 0.30 and 0.40, separation occurs at the maximum value; (c) is less than 0.30, then separation does not occur.

9.1 RESULTS FOR SCHUBAUER'S ELLIPTIC CYLINDER

Figures 31 and 32 show the results for Schubauer's elliptic cylinder [43], which has a 3.98-inch minor axis, D. The experimental pressure distribution was given at a free-stream velocity of $u_\infty = 60$ feet per second, corresponding to a Reynolds number of $R_D = 1.18 \times 10^5$. The extent of the transition region was between $x/D = 1.25$ and $x/D = 2.27$, and experimental separation was indicated at $x/D = 2.91$.

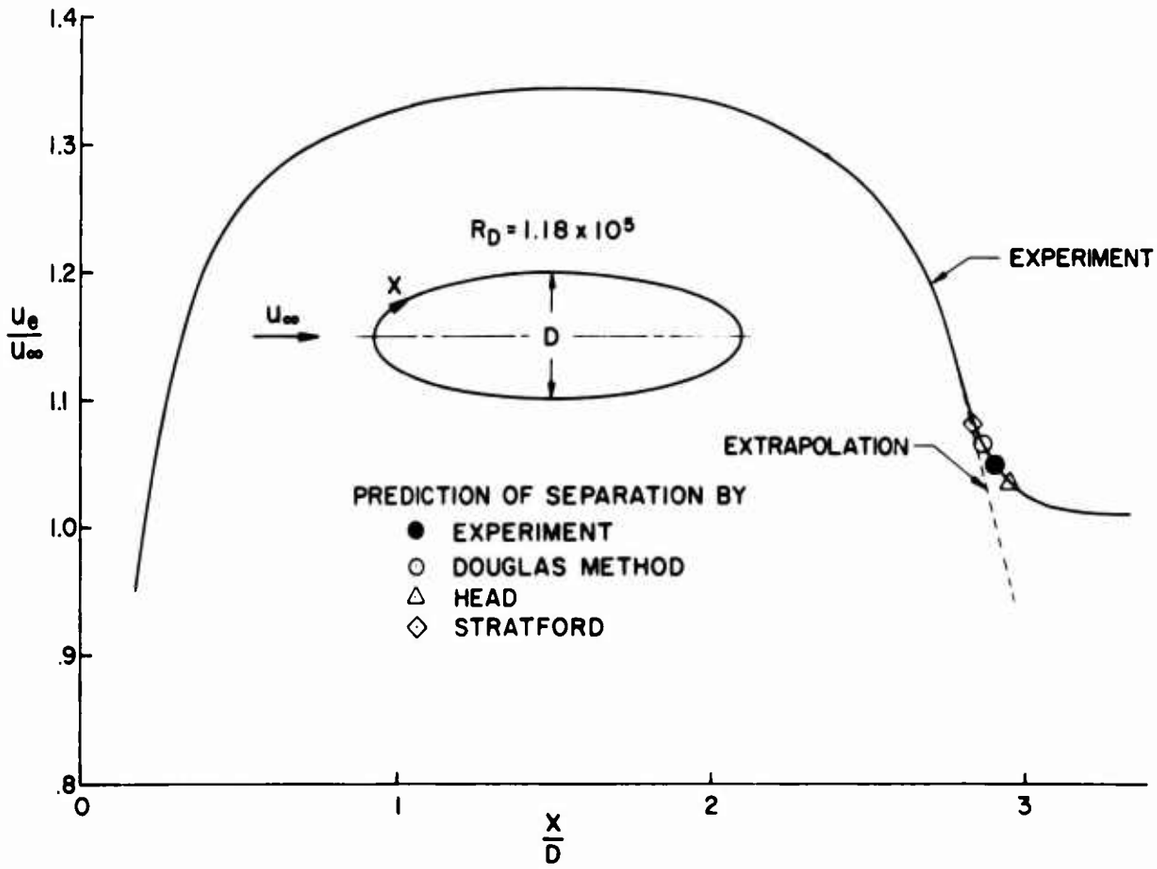

Figure 31. A comparison of predicted separation points with experiment for Schubauer's elliptic cylinder, $R_D = 1.18 \times 10^5$.

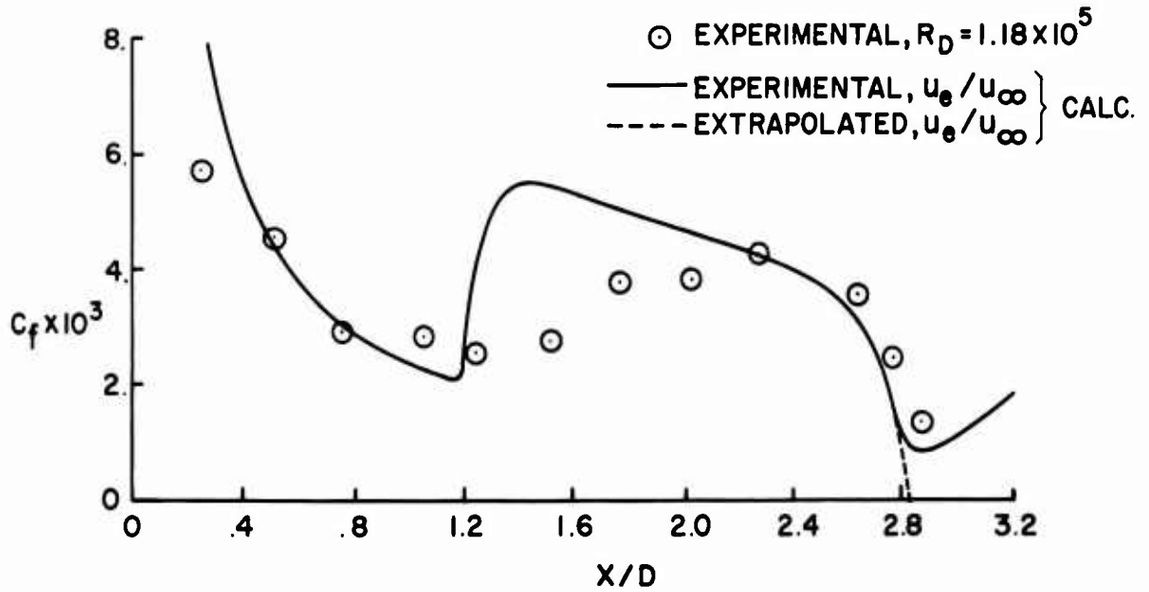

Figure 32. Comparison of calculated and experimental local skin-friction coefficients for Schubauer's elliptic cylinder [43]. The calculations were made by the Douglas boundary-layer method.

In the calculations the transition point was assumed at $x/D = 1.25$. Figure 31 shows the results. It is interesting to note that while three methods predicted separation, the fourth method, Goldschmiedt's method, did not predict any separation.

Figure 32 shows a comparison of calculated and experimental local skin-friction values. The calculations were made by using the Douglas boundary-layer method. It is important to note that when the experimental pressure distribution was used, the local skin-friction coefficient began to increase near separation due to the pressure distribution which was distorted by the flow separation. However, when the calculations were repeated by using an extrapolated velocity distribution which could be obtained by an inviscid method, the skin friction went to zero at $x/D = 2.82$.

Figure 33 shows a comparison of calculated and experimental velocity profiles at various x/D locations for the same body. In general, the agreement for both laminar and turbulent boundary layers seems to be quite satisfactory.

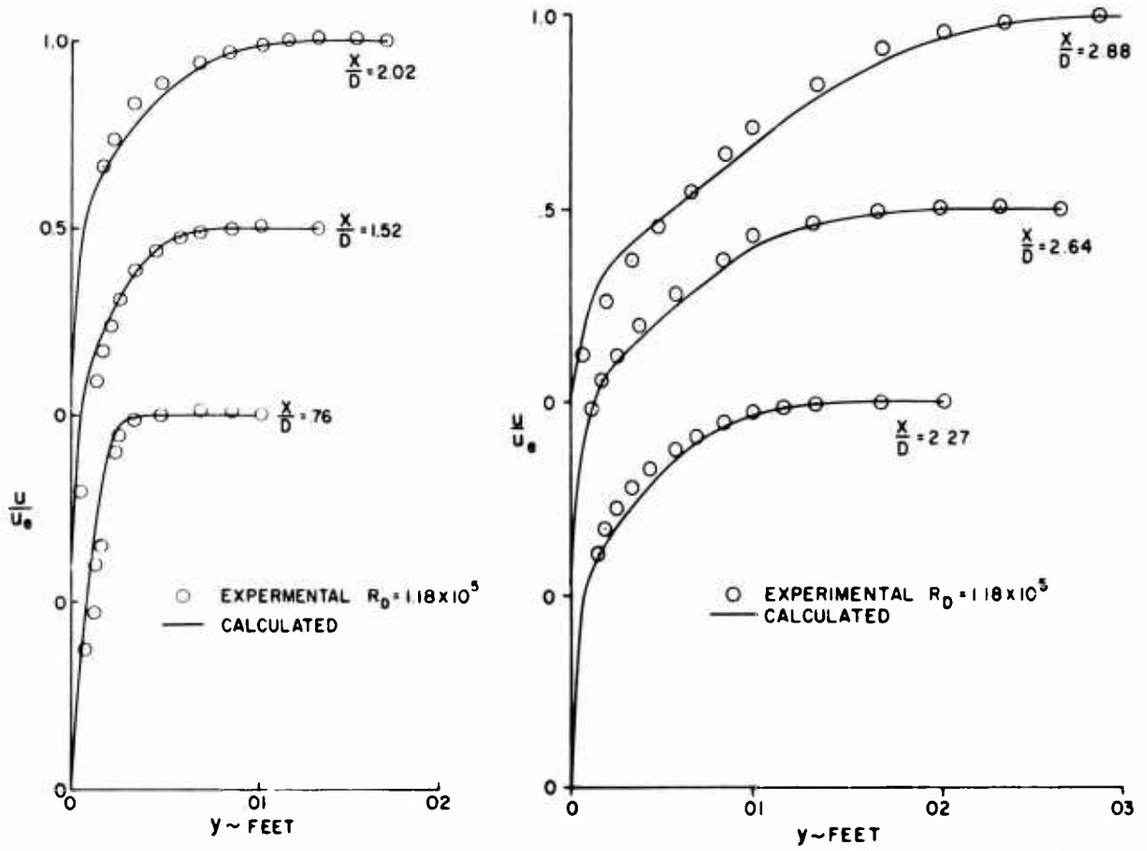

Figure 33. Comparison of calculated and experimental velocity profiles for Schubauer's elliptic cylinder [43]. The calculations were made by the Douglas boundary-layer method.

9.2 RESULTS FOR ROSHKO'S CIRCULAR CYLINDER

Figure 34 shows the predicted separation points together with the experimental points for Roshko's circular cylinder [44] for two diameter Reynolds numbers, $R_D = 6.7 \times 10^5$ and 8.4×10^6, that are within the so-called "supercritical" and "transcritical" Reynolds number ranges.

According to Roshko, at $R_D = 6.7 \times 10^5$ a separation bubble exists for angles between 100 and 120 degrees. This can be inferred from the pressure distribution. However, it is difficult to find the exact location of turbulent reattachment point. Also, the turbulent separation point in this case must be very close to the reattachment point. Thus, the extent of attached turbulent flow is probably very small,possibly between 115 and 120 degrees.

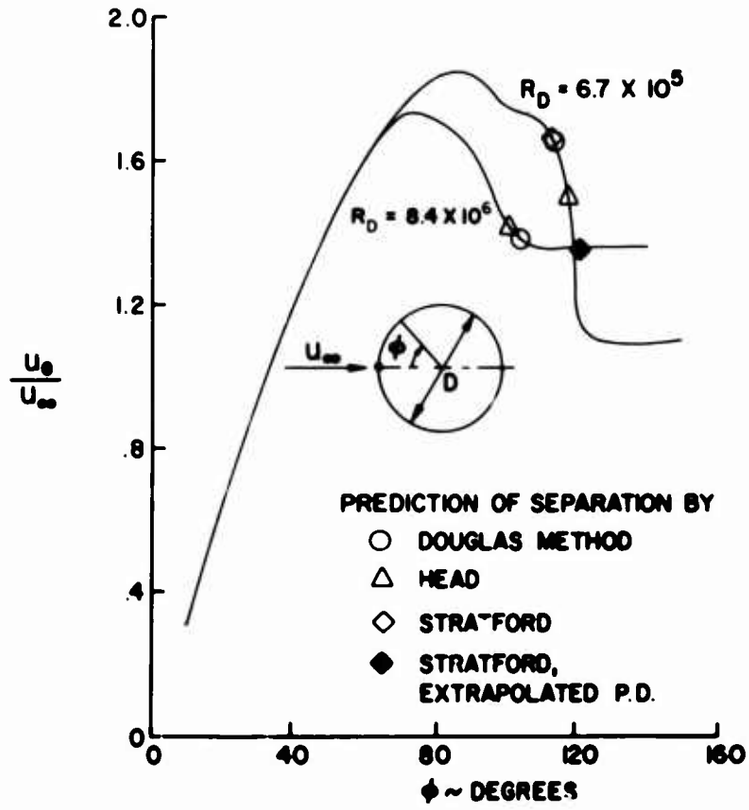

Figure 34. Comparison of predicted separation points with experiment for Roshko's circular cylinder [44].

At higher Reynolds number, $R_D = 8.4 \times 10^6$, on the other hand, the laminar separation region is much smaller and the extent of the turbulent flow region is fairly large as evident from the forward movement of the minimum pressure point and the smaller pressure peak.

For both Reynolds numbers, Goldschmied's method did not predict separation. On the other hand, in both cases the Douglas boundary-layer method and Head's method predicted separation. For $R_D = 6.7 \times 10^5$, Stratford's method predicted separation and for $R_D = 8.4 \times 10^6$ it did not. In the latter case $F(x)$ was less than 0.2. However, when the velocity distribution was extrapolated (see figure 35), then separation was predicted.

Figure 35 shows the variation of shape factor for the experimental and extrapolated velocity distributions at $R_D = 8.4 \times 10^6$. The calculations were made by Head's method. As expected with the extrapolated velocity distribution

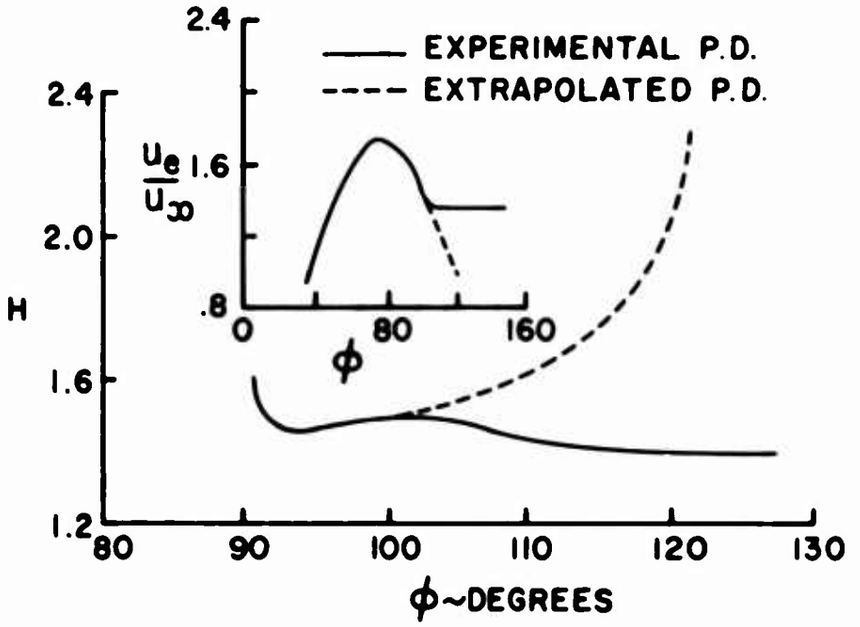

Figure 35. Variation of shape factor with two pressure distributions for Roshko's circular cylinder [44]. Calculations were made by Head's method for $R_D = 8.4 \times 10^6$.

(which is similar to inviscid velocity distribution), the shape factor quickly increases close to separation. On the other hand, with the experimental velocity distribution, the shape factor reaches a maximum and then starts to decrease.

9.3 RESULTS FOR SEVERAL AIRFOILS

Figures 36 through 41 show the results obtained for several airfoils where flow separation was observed. The results for the pressure distribution of Schubauer and Klebanoff are shown in figure 36. This pressure distribution was observed over an airfoil-like body at a Reynolds number per foot of 0.82×10^6. The experimental separation point was given at 25.7 ± 0.2 feet. The predictions of all methods are quite good.

As shown in figure 37, agreement between the Douglas boundary-layer method and experiment is also very good for Newman's airfoil. On the other hand, the other methods predict an early separation.

For the pressure distributions of figures 38 through 41, the experimental separation points were not given. The results show that, except at very high angles of attack, both boundary-layer methods predict separation at approximately the same locations and generally close to the characteristic "flattening" in the pressure distribution curves. Stratford's method predicts a slightly earlier separation than that given by the boundary-layer methods. On the other hand, Goldschmied's method shows results that are somewhat inconclusive, predicting early separation in some cases and late separation in others.

9.4 RESULTS FOR AXISYMMETRIC FLOWS

For axisymmetric flows, Head's and Stratford's methods cannot be used to predict the position of separation in their present form. For this reason only the Douglas boundary-layer method and Goldschmied's method were used to predict the separation points such flows.

Table 6 shows the results for the Murphy bodies [36]. The experimental separation points were obtained by the "oil-talc" technique. The calculated separation points by the Douglas boundary-layer method were obtained by extrapolating the skin-friction values to zero. The agreement is excellent.

Table 6

COMPARISON OF CALCULATED AND EXPERIMENTAL SEPARATION POINTS FOR THE BODIES OF REVOLUTION OF MURPHY [36]

Tail Shape	$R_L \times 10^6$	x_{sep} (inches)		
		Experiment	Douglas Method	Goldschmiedt Method
A-2	6.0	59.1	59.4	no separation
C-2	6.0	58.3	58.3	no separation
C-4	6.6	no separation	no separation	no separation

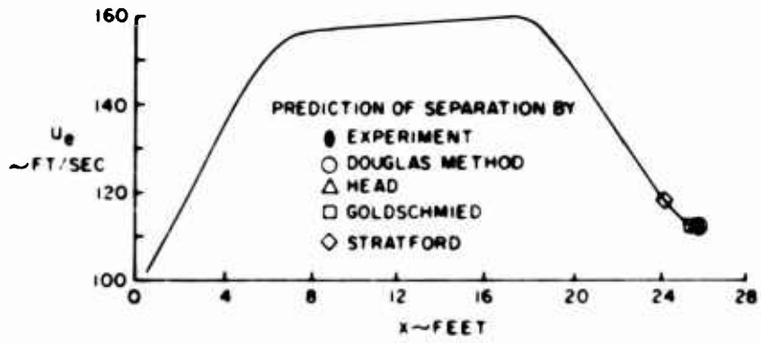

Figure 36. Comparison of predicted separation points with experiment for the airfoil-like body of Schubauer and Klebanoff [45].

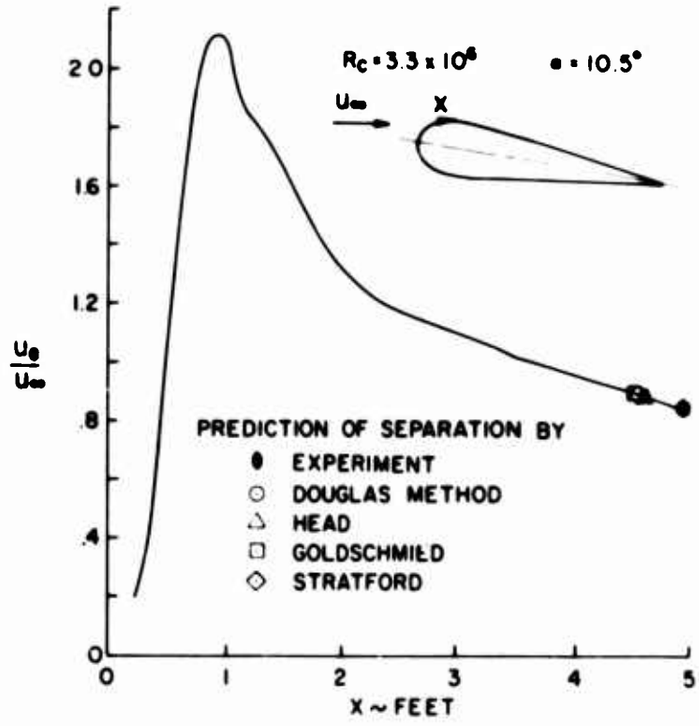

Figure 37. Comparison of predicted separation points with experiment for Newman's airfoil [39].

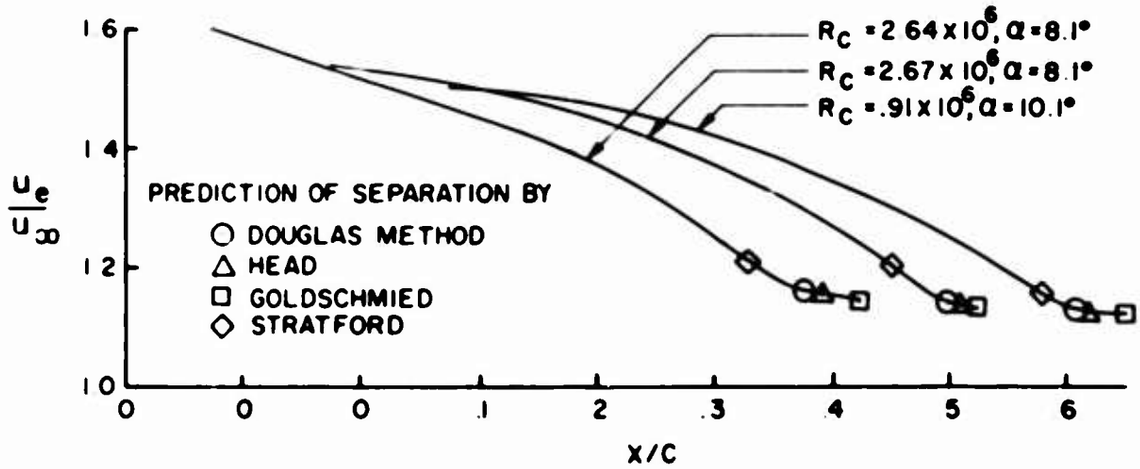

Figure 38. Predicted separation points for the experimental pressure distribution on the NACA 65(216)-222 airfoil [46].

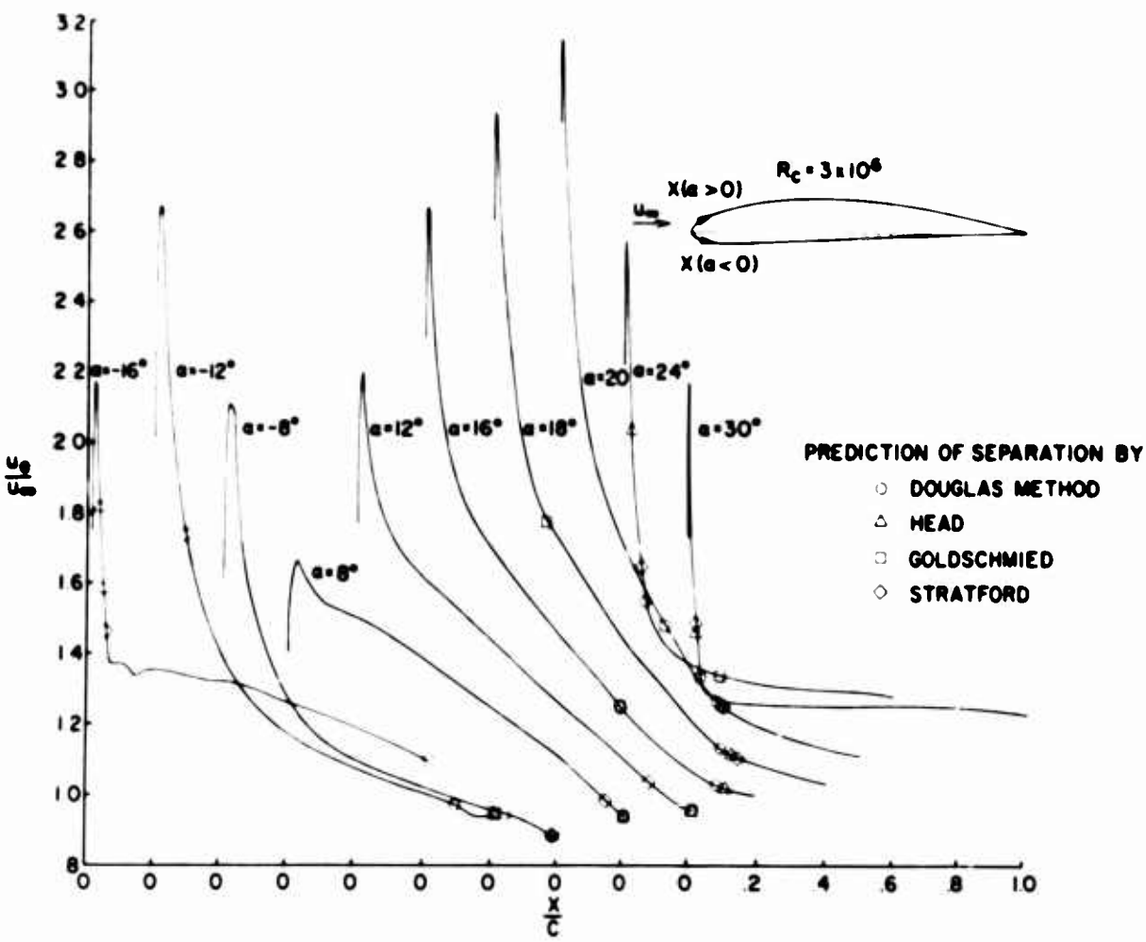

Figure 39. Predicted separation points for the experimental pressure distribution on the NACA 4412 airfoil [26].

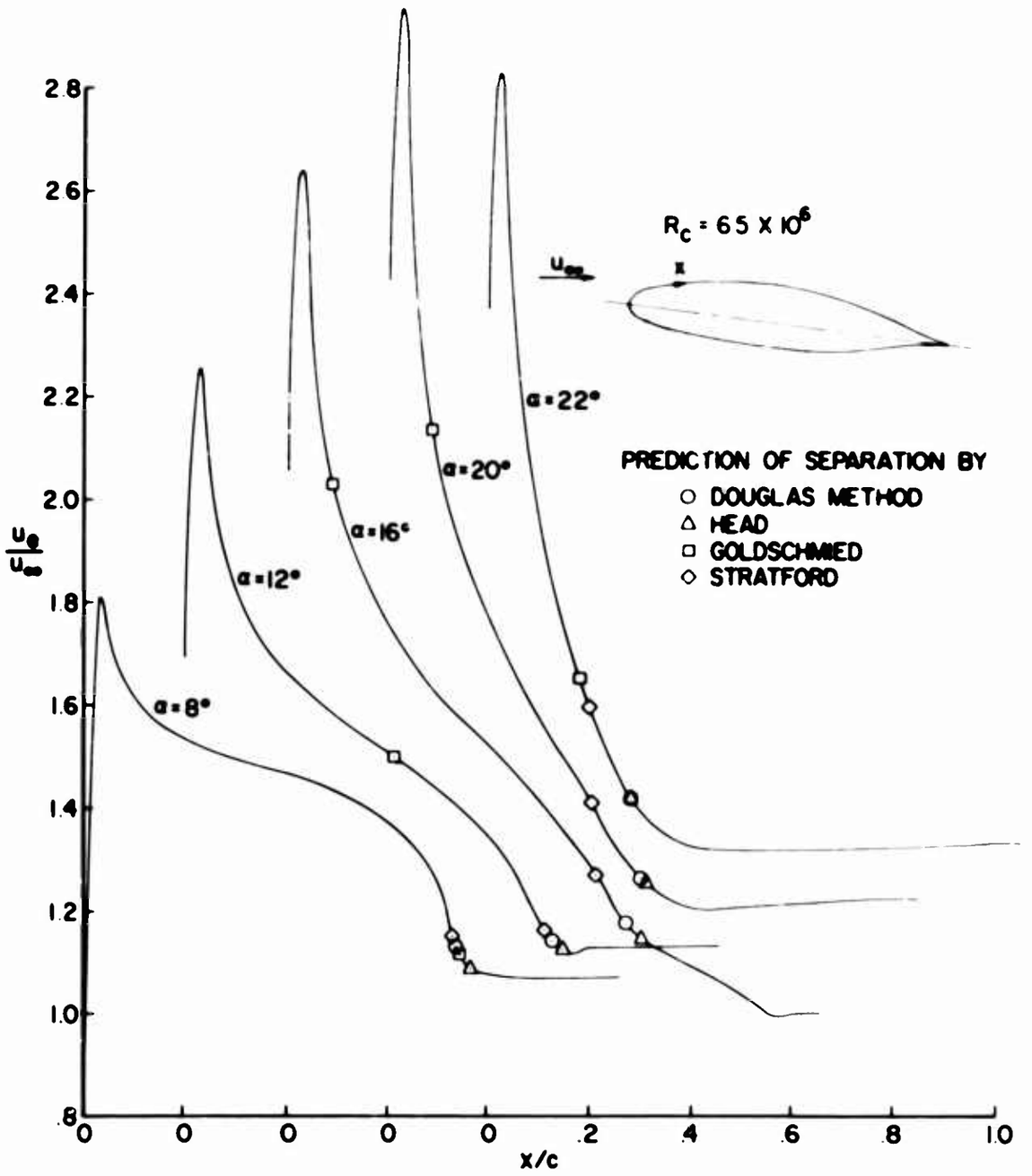

Figure 40. Predicted separation points for the experimental pressure distribution on the NACA 66,2-420 airfoil [30].

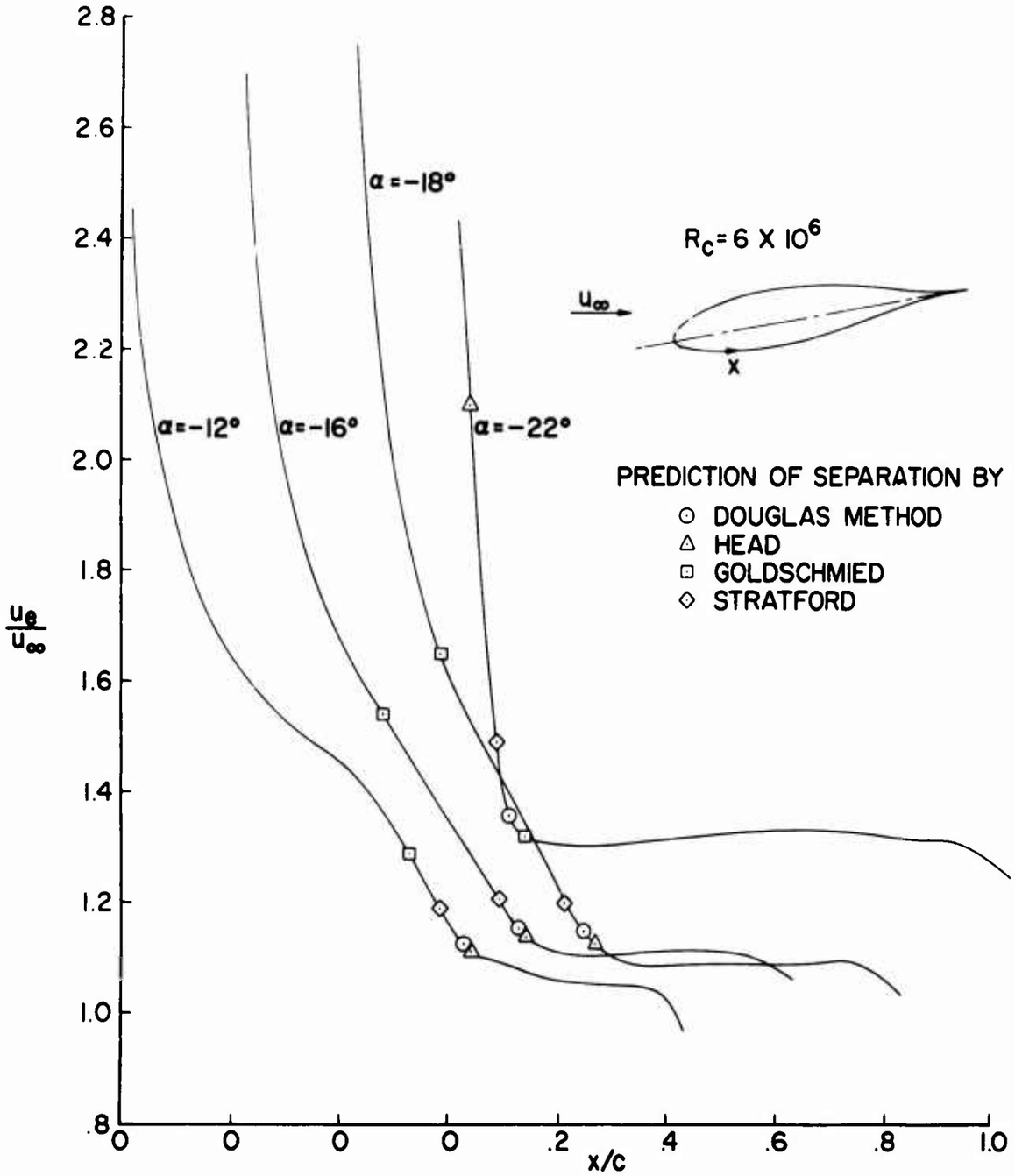

Figure 41. Predicted separation points for the experimental pressure distribution on the NACA 65,2-421 airfoil [47]. (a) Negative angles of attack.

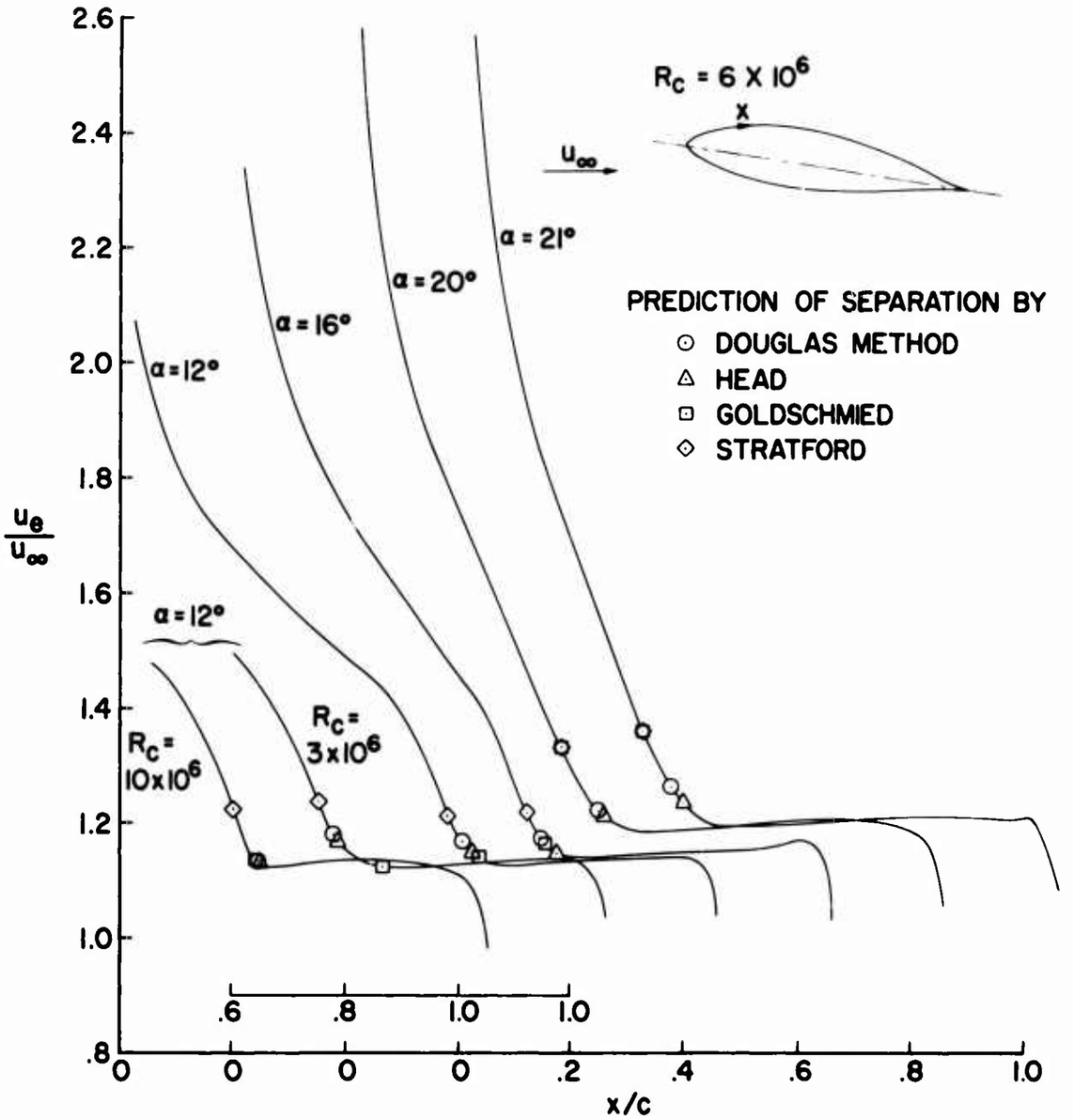

Figure 41. Concluded. (b) Positive angle of attack.

10.0 CONCLUDING REMARKS

The accuracy of calculating the total drag coefficients of two-dimensional and axisymmetric bodies, and the accuracy of predicting the location of turbulent boundary-layer separation in incompressible flows past such bodies has been studied.

In the drag calculations boundary-layer development was calculated by using the Douglas boundary-layer method. The inviscid pressure distribution was obtained by the Douglas Neumann method when the experimental pressure distribution was not given. In the boundary-layer calculations the location of transition was obtained by using Michel's or Granville's methods when it was not known. For two-dimensional bodies the total drag coefficient was calculated by using Squire-Young's formula. Jones' formula gave almost identical results. For axisymmetric bodies, the total drag coefficient was calculated by using Granville's formula. Similar results were also obtained by Young's formula.

Based on the calculations reported here, the following remarks can be made on the accuracy of calculating the total drag coefficient and the location of turbulent boundary-layer separation of two-dimensional and axisymmetric bodies:

1. The total drag coefficient of two-dimensional bodies can be calculated quite accurately provided that the angle of incidence is small, $\alpha < 6^{o}$. Although the boundary-layer development can be calculated very accurately by the Douglas boundary-layer method, at high angles of incidence ($\alpha > 6^{o}$) without boundary-layer separation, use of the Squire-Young formula introduces an error into the drag calculations. This is to be expected since the Squire-Young formula is applicable only to a symmetrical wake. With increasing incidence, the assumption of a "symmetrical" wake becomes worse. As an example, in figure 42 we show the variation of $(C_{D_{exp}} - C_{D_{cal}})$ with angle of incidence for three airfoils.

   The calculated results also indicate that (see figure 15) the drag of a body can be calculated at high Reynolds numbers. This is quite significant since, although good agreement was obtained at lower

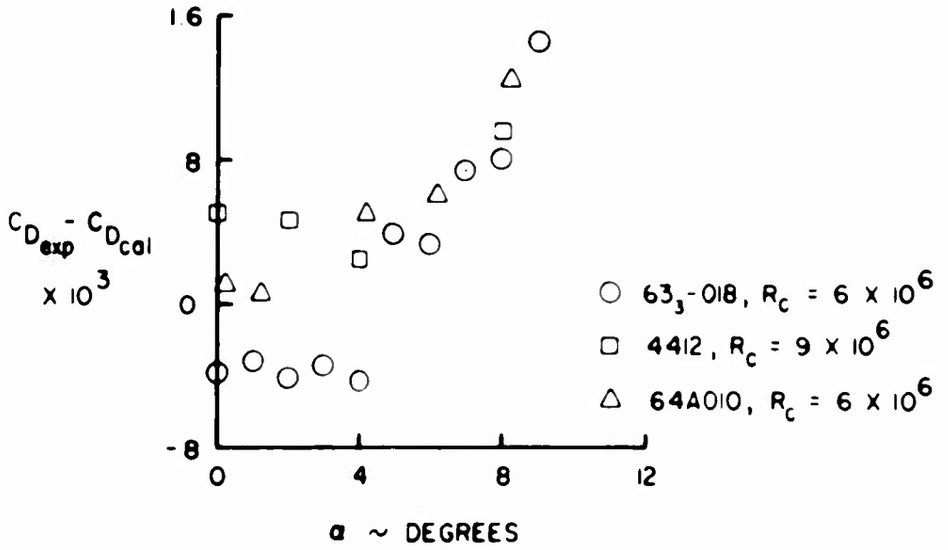

Figure 42. Variation of $C_{D_{exp}} - C_{D_{cal}}$ with angles of incidence for three airfoils.

Reynolds numbers ($R_c < 9 \times 10^6$) in the study described in reference 4, the agreement was poor at high Reynolds numbers, and the discrepancy was attributed to the inaccuracy of calculating turbulent boundary layers at high Reynolds numbers.

Figure 43 presents a comparison of calculated and experimental total-drag coefficients for angles of incidence less than 6°. Considering the various factors that influence the calculations, the results are very good. The rms error based on the 57 calculated drag values is 2.9%. It is interesting to note that in the previous study, the rms error was 2.7%. However, this was obtained by multiplying the Squire-Young formula by an empirical constant of 1.1 (for one surface). In the present study, no need for such a "correlation" constant was necessary.

2. The total-drag coefficients of axisymmetric bodies can be calculated with less accuracy than the total drag coefficients of the two-dimensional bodies. For axisymmetric bodies, the calculations show a great sensitivity to the choice of tail end location on the body and to

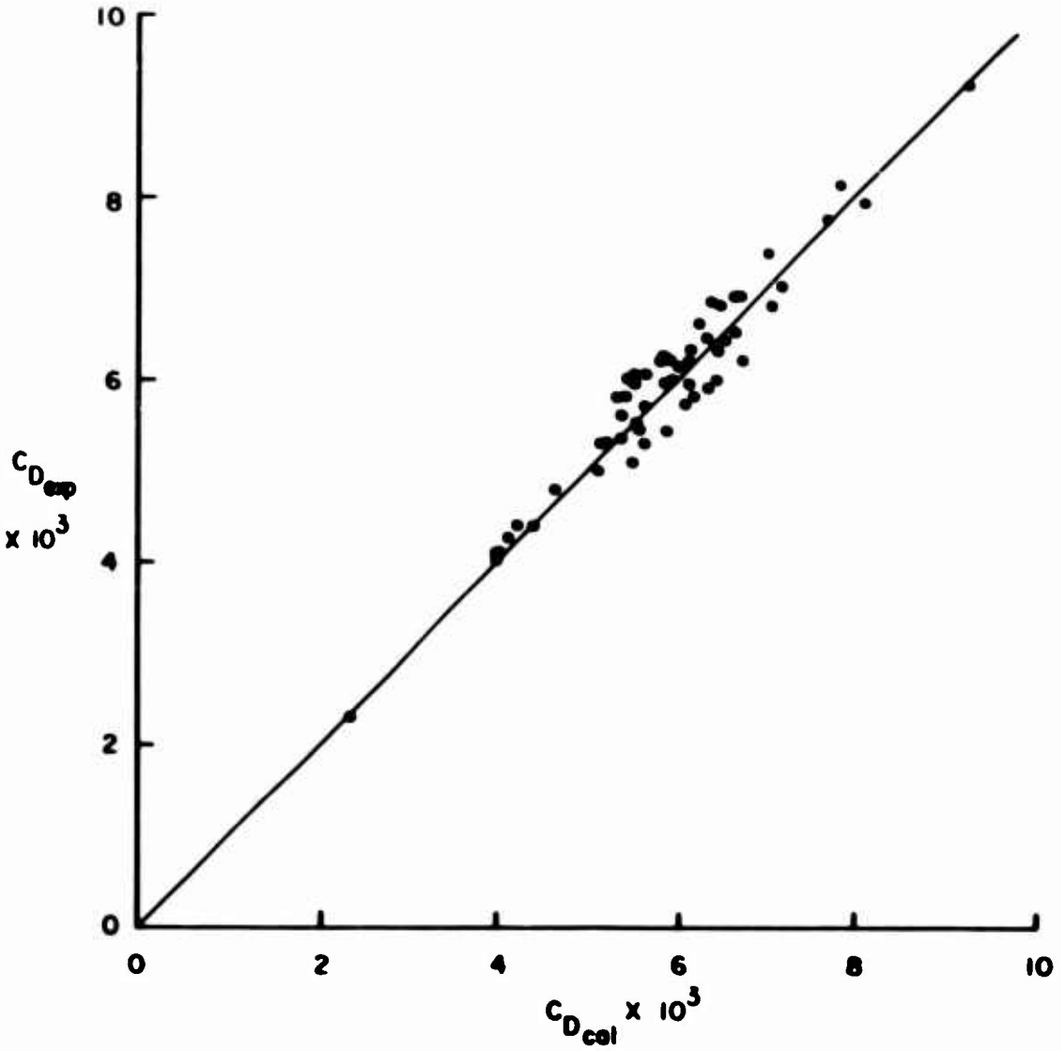

Figure 43. Comparison of calculated and experimental results for two-dimensional bodies. The results are shown for 57 drag values at angles of incidence less than 6 degrees.

the use of inviscid pressure distributions in the drag calculations. Although with viscous correction to the pressure distribution, the sensitivity was somewhat reduced, further work should be done in this area. This will later be discussed in Section 11.

The results also indicate that in applying either Granville's or Young's formulas, it is necessary to use the two-dimensional definition of momentum area, θ_a. Furthermore, as in two-dimensional bodies, the results indicate that the boundary-layer development can be calculated quite accurately at high Reynolds numbers on axisymmetric bodies. See figure 27.

3. The location of turbulent boundary-layer separation on two-dimensional bodies can be calculated quite satisfactorily by the Douglas boundary-layer method, Head's method and Stratford's method. Goldschmied's method is inconclusive. This is probably due to the very questionable assumption about the total pressure at the edge of the viscous sublayer.

   The results indicate that both boundary-layer methods predict the location of separation at approximately the same location. However, in some cases the predictions of the Douglas method agree better with experiment than the predictions of Head's method. Stratford's method is slightly conservative in its prediction.

4. The location of turbulent boundary-layer separation on axisymmetric bodies can be calculated quite accurately by the Douglas boundary-layer method. Head's method and Stratford's method in their present form are not applicable to such flows. The predictions of Goldschmied's method, although this method is also applicable to axisymmetrical flows, did not agree well with experiment.

11.0 FUTURE WORK

At the writing of this report, the studies concerning the drag calculations are partially completed and further work is needed to complete the studies.

As it was described in Section 6.1, there are three different approaches one can use to calculate the total drag of a body. In this report only one approach was studied completely. According to this approach the total drag of a body was calculated by a formula once the development of the boundary layer at the tail end of the body was calculated. This approach worked well for two-dimensional bodies provided that the angle of incidence is small. The approach, on the other hand, did not work as well for bodies of revolution. The formulas showed a great sensitivity to the location of the tail end and to the use of inviscid pressure distribution.

It appears from the results obtained by the first approach that in order to calculate the total drag of two-dimensional bodies at higher angles of incidence (without any boundary-layer separation, and the total drag of bodies of revolution at zero incidence at zero incidence) it is necessary to carry the calculations from the trailing edge into the wake. This is the second approach discussed in Section 6.1.

The wake calculations can be made by identifying two regions. The first is a region very close to the trailing edge. Here there are two boundary layers back to back, and not much is known about the way they interact. According to reference 48, the extent of this region from the trailing edge is about 7δ where δ is the boundary-layer thickness at the trailing edge. Recent calculations for this region reported by Bradshaw appear to give satisfactory results for the case of symmetrical airfoil wakes [48]. For nonsymmetrical wakes (the wakes of airfoils at an angle of incidence or airfoils with camber), more experimental wake data showing the variation of Reynolds shear stress and velocity profiles are needed before the calculations can be made for such cases.

The second region is the region far beyond the trailing edge, where the effects of trailing edge are negligible. Here the calculations seem to be somewhat easier to perform, and part of the efforts in the study reported here

were devoted to the accuracy of calculating turbulent wake profiles in this region. The calculations were made by using the same eddy-viscosity expression that is used in the Douglas boundary-layer method. That is,

$$\varepsilon = \alpha \left| \int_0^{\delta} (u_e - u)dy \right| \gamma \tag{11.1}$$

Several preliminary calculations with α = 0.0168 and 0.0336 showed that predicted results improved slightly with α = 0.0336, a value slightly lower than the value commonly suggested in the literature (α = 0.036). The calculated results are shown in figure 44 for the experimental data of Hill et al. [49]. The agreement is fair. More comparisons with experiment are necessary in order to study the accuracy of the extension of the Douglas boundary-layer method to such flows.

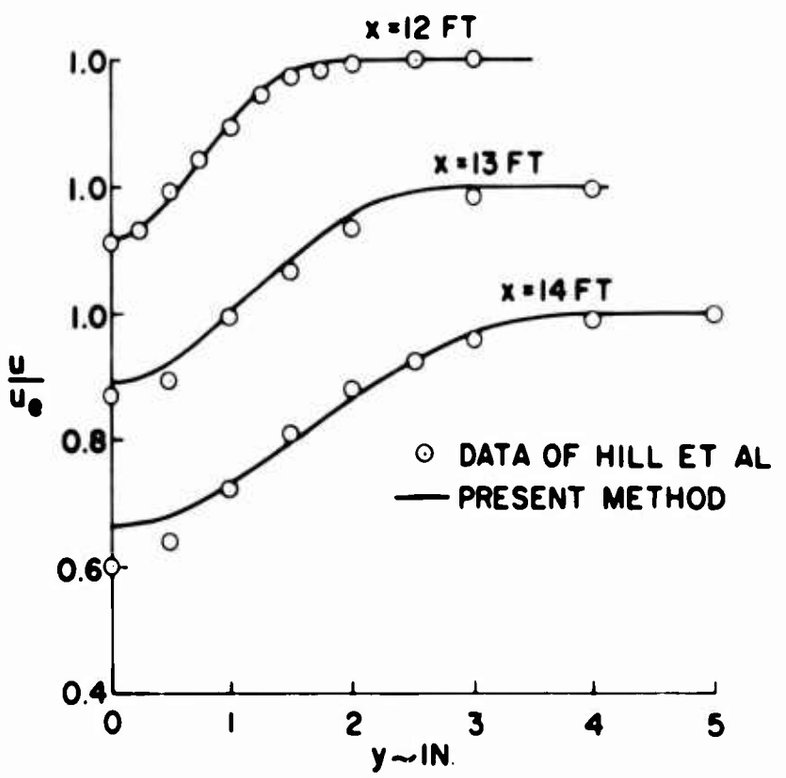

Figure 44. Comparison of calculated and experimental wake profiles in adverse pressure gradients.

A third approach by which the total drag of a body can be calculated is one in which the pressure drag and skin-friction drag are calculated separately. In an inviscid flow, there is no pressure drag. It can be obtained as follows:

1. Calculate the inviscid pressure distribution on the basic body.

2. Calculate the boundary-layer development for the pressure distribution of 1.

3. Modify the basic shape by adding on the displacement thickness and calculate a pressure distribution for the new effective shape. The body is now open ended and yields a pressure force.

It should be pointed out, however, that in performing the boundary-layer calculations it may also be necessary to carry the calculations into the wake, although not too far (possibly 7δ where δ is the boundary-layer thickness at the tail end). The region of the tail end of the body is a "problem" region and careful attention must be paid to the assumptions made in this region.

An alternate method which is not rigorous but may have essentially the same accuracy with much more economical calculation time is as follows:

1. Calculate the inviscid pressure distribution of the basic body.

2. Calculate the boundary-layer development for the pressure distribution of 1.

3. By means of well-known relations, recalculate the inviscid flow about the original body but now with outflow through the walls sufficient to displace the inviscid streamlines by an amount equal to the displacement thickness. Now there is a net yield of fluid and the streamlines do not close.

4. The Douglas Neumann method solves the flow field problem by using surface source-sink distribution. Then the pressure drag correction is equal to this inviscid momentum flux which is

$$\Delta D = 2\pi\rho V_\infty \int_{\text{surface}} \sigma dS \qquad (11.2)$$

where σ is the surface source density. It is believed that when the total drag coefficients are calculated by the third approach, it is not necessary to repeat the boundary-layer calculations for the viscous-corrected inviscid pressure distribution. The latter method of the third approach has two significant computational advantages. Potential flow solutions are always made for the same body so that the influence coefficient matrix is never changed, even if one considers several angles of attack. The changes occur only in the right-hand column of the matrix equation in order to account for the effective outflow through the surface. In the first method of the third approach, each time the boundary layer is changed, the entire inviscid problem must be solved anew. The second significant advantage is that it is much easier to compute $\int \sigma dS$ over the body than to determine the net pressure drag component.

This method should be equally valid for axisymmetric or two-dimensional flow. Because the potential flow problem is elliptic, flow processes downstream of the shape can influence results upstream. Therefore, there remains the possibility that the near wake flow must still be solved if the highest accuracy is desired.

In the calculations reported here, the position of transition on the airship for the case of $R_L = 94 \times 10^6$, was predicted at the 45%-chord point. The actual transition point was approximately at 5%-chord point. According to the study reported by Granville, the methods of Michel and Granville are not satisfactory for predicting the position of transition on axisymmetric bodies [50]. This is due to another variable that enters into the transition calculations. It is the body shape. It enters directly because the shape has a direct stretching or shrinking effect on the boundary layer in addition to determining the pressure distribution. Therefore, it should not be expected that correlation methods, especially Michel's, should be as accurate as for two-dimensional flows. The e^9 method is indeed a correlation method but it bypasses the body of revolution difficulty. It attempts to trace carefully the growth of various Tollmien-Schlichting waves along the body and the procedure is equally applicable to axisymmetric and two-dimensional

flows. Recently, a very general computer program has been developed that first computes accurate laminar boundary layers for numerous stations along a body for both axisymmetric and two-dimensional flows. The stability of the boundary layer is computed for a variety of disturbance frequencies for the boundary-layer profile computed at several stations. Then the growth of the worst frequency is computed. The method is described in reference [51], and it seems to promise rather good precision. However, it has never been carefully studied for axisymmetric flows, partly because the labor is large and partly because the computing time is considerable. Since this treatment is the most promising lead now known, it should be explored to make a good assessment of its accuracy for axisymmetric flows. There is an adequate supply of suitable experimental data for such a study [52].

12.0 ACKNOWLEDGMENTS

The authors would like to acknowledge Kalle Kaups for helpful discussions during the development of this work.

13.0 REFERENCES

1. Cebeci, T.; and Smith, A.M.O.: A Finite-Difference Solution of the Incompressible Turbulent Boundary-Layer Equations by an Eddy-Viscosity Concept. Proceedings of the 1968 AFOSR-IFP-Stanford Conference on Computation of Turbulent Boundary Layers, Vol. 1, Stanford University, pp. 346-355.
2. Hess, J.L.; and Smith, A.M.O.: Calculation of Potential Flow About Arbitrary Bodies. Progress in Aeronautical Sciences, Vol. 8, Pergamon Press, New York, 1966.
3. Schlichting, H.: Boundary-Layer Theory. McGraw Hill, New York, 1960.
4. Cebeci, T.; and Smith, A.M.O.: Calculation of Profile Drag of Airfoils at Low Mach Numbers. J. of Aircraft, Vol. 5, No. 6, Nov-Dec 1968.
5. Granville, P.S.: The Calculation of the Viscous Drag of Bodies of Revolution. The David W. Taylor Model Basin Report 849, July 1953.
6. Nark, T.C.: Theoretical Prediction of Airfoil Drag Polars. Paper presented at Society of Automotive Engineers Business Aircraft Meeting, Wichita, Kansas, 3-5 April 1968.
7. Nash, J.F.; Osborne, J.; and MacDonald, A.G.J.: A Note on the Prediction of Aerofoil Profile Drag at Subsonic Speeds. Aero Rept 1196, National Physical Lab., England, May 1966.
8. Young, A.D.: The Calculation of the Total and Skin-Friction Drags of Bodies of Revolution at Zero Incidence. R and M Rept No. 1874, 1939.
9. Thwaites, B.: Approximate Calculation of the Laminar Boundary Layer. The Aeronautical Quarterly, Nov 1949.
10. Michel, R.: Etude de la transition sur les profiles d'aile; establissement d'un critere de determination du point de transition et calcul de la trainee de profile incompressible. O.N.E.R.A. Rept 1/1578A, July 1951. Also Pub. No. 58, 1952.
11. Head, M.R.: Entrainment in the Turbulent Boundary Layer. R and M 3152, 1960, Aeronautical Research Council, England.
12. Cebeci, T.; and Smith, A.M.O.: A Finite-Difference Method for Calculating Compressible Laminar and Turbulent Boundary Layers. J. of Basic Eng., Vol. 92, No. 3, pp. 523-535, Sept 1970.

13. Cebeci, T.: Laminar and Turbulent Incompressible Boundary Layers on Slender Bodies of Revolution in Axial Flow. J. of Basic Eng., Vol. 92, No. 3, pp. 545-554, Sept 1970.

14. Simpson, R.L.; Kays, W.M.; and Moffat, R.J.: The Turbulent Boundary Layer on a Porous Plate: An Experimental Study of the Fluid Dynamics with Injection and Suction. Rept. No. HMT-2, Stanford University, 1967.

15. Julien, H.L.; Kays, W.M.; and Moffat, R.J.: The Turbulent Boundary Layer on a Porous Plate: Experimental Study of the Effects of a Favorable Pressure Gradient. Rept. No. HMT-4, Stanford University, 1969.

16. Coles, D.E.: The Turbulent Boundary Layer in a Compressible Fluid. Rand Corporation Rept. P-2417, 1961.

17. Van Driest, E.R.: On Turbulent Flow Near a Wall. J. of Aeronautical Sci., Vol. 23, No. 11, Nov 1956.

18. Cebeci, T.: The Behavior of Turbulent Flow Near a Porous Wall with Pressure Gradient. Douglas Aircraft Co. Rept. No. 70014, 1969.

19. Coles, D.: Measurements in the Boundary Layer on a Smooth Flat Plate in Supersonic Flow. I. The Problem of the Turbulent Boundary Layer. Jet Propulsion Lab. Rept. No. 20-69, June 1953.

20. Kline, S.J.; Morkovin, M.V.; Sovran, G.; and Cockrell, D.S.: Computation of Turbulent Boundary Layers. AFOSR-IFP-Stanford Conference, Vol. II, 1968.

21. Thomann, H.: Effect of Streamwise Wall Curvature on heat Transfer in a Turbulent Boundary Layer. J. of Fluid Mechanics, Vol. 33, Pt. 2, pp. 283-292, 1968.

22. Bradshaw, P.: The Analogy Between Streamline Curvature and Buoyancy in Turbulent Shear Flow. NPL Aero Rept 1231, 1967.

23. Smith, A.M.O.: Transition, Pressure Gradient, and Stability Theory. Proceedings of 9th International Congress of Applied Mechanics, Brussels, Belgium, Vol. 4, p. 234, 1956.

24. Thwaites, B.: Incompressible Aerodynamics. Oxford University Press, Oxford, England, 1960.

25. Braslow, A.L.; and Visconti, F.: Investigation of Boundary-Layer Reynolds Number for Transition on a NACA $65_{(215)}$-114 Airfoil in the Langley Two-Dimensional Low Turbulence Pressure Tunnel. NACA TN 1704, 1948.

26. Pinkerton, R.: Pressure Distribution Over the Midspan Section of the NACA 4412 Airfoil. Rept 563, 1936.
27. Abbott, I.H.; and VonDoenhoff, A.E.: Theory of Wing Sections. Dover Publications Inc., June 1958.
28. Stivers, L.S.: Effects of Subsonic Mach Number on the Forces and Pressure Distributions on Four NACA 64A-Series Airfoil Sections at Angles of Attack as High as 28°. NACA TN 3162, 1954.
29. Brebner, C.G.; and Bagley, J.A.: Pressure and Boundary-Layer Measurements on a Two-Dimensional Wing at Low Speed. ARC R and M No. 2886, 1956.
30. Hood, M.J.; and Anderson, J.L.: Tests of an NACA 66,2-420 Airfoil of 5-Foot Chord at High Speed. NACA Rept No. ACR 546, 1942.
31. Wetmore, J.W.; Zalovick, J.A.; and Platt, R.C.: A Flight Investigation of the Boundary-Layer Characteristics and Profile Drag of the NACA 35-215 Laminar Flow Airfoil at High Reynolds Numbers. NACA Waretime Rept L-532, 1941.
32. McCullough, G.B.; and Gault, D.E.: Examples of Three Representative Types of Airfoil-Section Stall at Low Speed. NACA TN 2502, 1951.
33. Amick, J.L.: Comparison of the Experimental Pressure Distribution on an NACA 0012 Profile at High Speeds with that Calculated by the Relaxation Method. NACA TN 2174, 1950.
34. Gertler, M.: Resistance Experiments on a Systematic Series of Streamlined Bodies of Revolution - For Application to the Design of High-Speed Submarines. Navy Department. DTMB Rept No. C-297, 1950.
35. Cornish, J.J., III; and Boatwright, D.W.: Application of Full Scale Boundary-Layer Measurements to Drag Reduction of Airships. Aerophysics Dept, Mississippi State University Research Rept No. 28, 1960.
36. Murphy, J.S.: The Separation of Axially Symmetric Turbulent Boundary Layers. Douglas Aircraft Co. Rept No. ES 17513, March 1954.
37. Stratford, B.S.: The Prediction of Separation of the Turbulent Boundary Layer. J. Fluid Mech., Vol. 5, pp. 1-16, 1959.
38. Goldschmied, F.R.: An Approach to Turbulent Incompressible Separation Under Adverse Pressure Gradients. J. Aircraft, Vol. 2, No. 2, pp. 108-115, 1965.
39. Newman, B.G.: Some Contributions to the Study of the Turbulent Boundary Layer Near Separation. Australian Dept Supply, Rept No. ACA-53, 1951.

40. Goldberg, P.: Upstream History and Apparent Stress in Turbulent Boundary Layers. M.I.T. Rept, May 1966.

41. Townsend, A.A.: The Behavior of a Turbulent Boundary Layer Near Separation. J. of Fluid Mech., Vol. 12, pp. 536-554, 1962.

42. Sandborn, V.A.; and Liu, C.Y.: On Turbulent Boundary-Layer Separation. J. of Fluid Mech., Vol 23, pp. 293-304, 1968.

43. Schubauer, G.B.: Air Flow in the Boundary Layer of an Elliptic Cylinder. NACA TR 652, 1939.

44. Roshko, A.: Experiments on the Flow Past a Circular Cylinder at High Reynolds Number. J. of Fluid Mech., Vol. 10, pp. 345-356, 1961.

45. Schubauer, G.B.; and Klebanoff, P.S.: Investigation of Separation of the Turbulent Boundary Layer. NACA TN 2133, Aug 1950.

46. Von Doenhoff, A.E.; and Tetervin, N.: Determination of General Relations for the Behavior of Turbulent Boundary Layers. NACA Rept 772, 1943.

47. Abbott, I.H.: Lift, Drag, and Pressure-Distribution Tests of Six Airfoil Models Submitted by Consolidated Aircraft Corporation as Sections of a Wing for the XB-36 Airplane. NACA MR 612, 1942.

48. Bradshaw, P.: Calculation of Boundary-Layer Development Using the Turbulent Energy Equation. V: Wakes Near a Trailing Edge. NPL Aero Rept 1285, Jan 1969.

49. Hill, P.G.; Schaub, V.W.; and Senoo, Y.: Turbulent Wakes in Pressure Gradients. J. of Applied Mech., pp. 518-524, Dec 1963.

50. Granville, P.S.: Comparison of Existing Methods for Predicting Transition from Laminar to Turbulent Flow on Bodies of Revolution. Naval Ship Research and Development Center, Hydromechanics Laboratory TN 111, August 1968.

51. Jaffe, N.A.; Okamura, T.T.; and Smith, A.M.O.: Determination of Spatial Amplification Factors and Their Application to Predicting Transition. AIAA J., Vol. 8, No. 2, pp. 301-318, Feb 1970.

52. Groth, E.E.: Boundary-Layer Transition on Bodies of Revolution. Northrop Aircraft Rept No. NAI-57-1162 (BLC-100), July 1957.

Unclassified

Security Classification

DOCUMENT CONTROL DATA - R&D

(Security classification of title, body of abstract and indexing annotation must be entered when the overall report is classified)

1 ORIGINATING ACTIVITY (Corporate author) Douglas Aircraft Company, McDonnell Douglas Corp., Long Beach, California	2a REPORT SECURITY CLASSIFICATION Unclassified 2b GROUP Aerodynamics

3 REPORT TITLE

Calculation of Viscous Drag and Turbulent Boundary-Layer Separation of Two-Dimensional and Axisymmetric Bodies in Incompressible Flows

4 DESCRIPTIVE NOTES (Type of report and inclusive dates)

Technical Report

5 AUTHOR(S) (Last name, first name, initial)

Cebeci, Tuncer
Mosinskis, G.J.

6 REPORT DATE November 1970	7a TOTAL NO OF PAGES 90	7b NO OF REFS 52
8a CONTRACT OR GRANT NO N00014-70-C-0099 b PROJECT NO c d	9a ORIGINATOR'S REPORT NUMBER(S) MDC J0973-01 9b OTHER REPORT NO(S) (Any other numbers that may be assigned this report)	

10 AVAILABILITY/LIMITATION NOTICES

This document has been approved for public release and sale; its distribution is unlimited.

11 SUPPLEMENTARY NOTES	12 SPONSORING MILITARY ACTIVITY Naval Ship Research and Development Center Department of the Navy Washington, D.C. 20007

13 ABSTRACT

This report studies the accuracy of calculating the total drag of two-dimensional and axisymmetric bodies and the accuracy of calculating the location of turbulent boundary-layer separation in flows past such bodies.

The drag calculations were made by using the Douglas boundary-layer method. This is an implicit finite-difference method applicable to both laminar and turbulent boundary layers. The method also accounts for the transverse curvature effects. In general, comparison of calculated and experimental drag coefficients for both two-dimensional and axisymmetric bodies are in good agreement with experiment.

The separation calculations were made by considering four different separation-prediction methods. They are the Douglas boundary-layer method, Head's method, Stratford's method and Goldschmied's method. Comparisons of calculated and experimental results for several flows indicate that prediction of separation by the first three methods is quite good.

DD FORM 1 JAN 64 1473 0101-807-6800

Unclassified

Security Classification

Unclassified
Security Classification

14 KEY WORDS	LINK A ROLE	LINK A WT	LINK B ROLE	LINK B WT	LINK C ROLE	LINK C WT
Boundary Layers						
Drag						
Transition						
Laminar Boundary Layers						
Turbulent Boundary Layers						
Separation						

INSTRUCTIONS

1. ORIGINATING ACTIVITY: Enter the name and address of the contractor, subcontractor, grantee, Department of Defense activity or other organization *(corporate author)* issuing the report.

2a. REPORT SECURITY CLASSIFICATION: Enter the overall security classification of the report. Indicate whether "Restricted Data" is included. Marking is to be in accordance with appropriate security regulations.

2b. GROUP: Automatic downgrading is specified in DoD Directive 5200.10 and Armed Forces Industrial Manual. Enter the group number. Also, when applicable, show that optional markings have been used for Group 3 and Group 4 as authorized.

3. REPORT TITLE: Enter the complete report title in all capital letters. Titles in all cases should be unclassified. If a meaningful title cannot be selected without classification, show title classification in all capitals in parenthesis immediately following the title.

4. DESCRIPTIVE NOTES: If appropriate, enter the type of report, e.g., interim, progress, summary, annual, or final. Give the inclusive dates when a specific reporting period is covered.

5. AUTHOR(S): Enter the name(s) of author(s) as shown on or in the report. Enter last name, first name, middle initial. If military, show rank and branch of service. The name of the principal author is an absolute minimum requirement.

6. REPORT DATE: Enter the date of the report as day, month, year, or month, year. If more than one date appears on the report, use date of publication.

7a. TOTAL NUMBER OF PAGES: The total page count should follow normal pagination procedures, i.e., enter the number of pages containing information.

7b. NUMBER OF REFERENCES: Enter the total number of references cited in the report.

8a. CONTRACT OR GRANT NUMBER: If appropriate, enter the applicable number of the contract or grant under which the report was written.

8b, 8c, & 8d. PROJECT NUMBER: Enter the appropriate military department identification, such as project number, subproject number, system numbers, task number, etc.

9a. ORIGINATOR'S REPORT NUMBER(S): Enter the official report number by which the document will be identified and controlled by the originating activity. This number must be unique to this report.

9b. OTHER REPORT NUMBER(S): If the report has been assigned any other report numbers *(either by the originator or by the sponsor)*, also enter this number(s).

10. AVAILABILITY/LIMITATION NOTICES: Enter any limitations on further dissemination of the report, other than those imposed by security classification, using standard statements such as:

(1) "Qualified requesters may obtain copies of this report from DDC."

(2) "Foreign announcement and dissemination of this report by DDC is not authorized."

(3) "U. S. Government agencies may obtain copies of this report directly from DDC. Other qualified DDC users shall request through _____."

(4) "U. S. military agencies may obtain copies of this report directly from DDC. Other qualified users shall request through _____."

(5) "All distribution of this report is controlled. Qualified DDC users shall request through _____."

If the report has been furnished to the Office of Technical Services, Department of Commerce, for sale to the public, indicate this fact and enter the price, if known.

11. SUPPLEMENTARY NOTES: Use for additional explanatory notes.

12. SPONSORING MILITARY ACTIVITY: Enter the name of the departmental project office or laboratory sponsoring *(paying for)* the research and development. Include address.

13. ABSTRACT: Enter an abstract giving a brief and factual summary of the document indicative of the report, even though it may also appear elsewhere in the body of the technical report. If additional space is required, a continuation sheet shall be attached.

It is highly desirable that the abstract of classified reports be unclassified. Each paragraph of the abstract shall end with an indication of the military security classification of the information in the paragraph, represented as *(TS)*, *(S)*, *(C)*, or *(U)*.

There is no limitation on the length of the abstract. However, the suggested length is from 150 to 225 words.

14. KEY WORDS: Key words are technically meaningful terms or short phrases that characterize a report and may be used as index entries for cataloging the report. Key words must be selected so that no security classification is required. Identifiers, such as equipment model designation, trade name, military project code name, geographic location, may be used as key words but will be followed by an indication of technical context. The assignment of links, roles, and weights is optional.

Security Classification